

Ana M. Franceschi
Dinko Franceschi
Editors

Hybrid PET/MR Neuroimaging

A Comprehensive Approach

Hybrid PET/MR Neuroimaging

Ana M. Franceschi • Dinko Franceschi
Editors

Hybrid PET/MR Neuroimaging

A Comprehensive Approach

 Springer

Editors

Ana M. Franceschi
Donald and Barbara Zucker School of Medicine
at Hofstra/Northwell, The Feinstein Institutes
for Medical Research
Manhasset, NY
USA

Dinko Franceschi
Stony Brook University Hospital
Stony Brook, NY
USA

ISBN 978-3-030-82366-5 ISBN 978-3-030-82367-2 (eBook)
<https://doi.org/10.1007/978-3-030-82367-2>

© The Editor(s) (if applicable) and The Author(s), under exclusive license to Springer Nature Switzerland AG 2022
This work is subject to copyright. All rights are solely and exclusively licensed by the Publisher, whether the whole or part of the material is concerned, specifically the rights of translation, reprinting, reuse of illustrations, recitation, broadcasting, reproduction on microfilms or in any other physical way, and transmission or information storage and retrieval, electronic adaptation, computer software, or by similar or dissimilar methodology now known or hereafter developed.

The use of general descriptive names, registered names, trademarks, service marks, etc. in this publication does not imply, even in the absence of a specific statement, that such names are exempt from the relevant protective laws and regulations and therefore free for general use.

The publisher, the authors, and the editors are safe to assume that the advice and information in this book are believed to be true and accurate at the date of publication. Neither the publisher nor the authors or the editors give a warranty, expressed or implied, with respect to the material contained herein or for any errors or omissions that may have been made. The publisher remains neutral with regard to jurisdictional claims in published maps and institutional affiliations.

This Springer imprint is published by the registered company Springer Nature Switzerland AG
The registered company address is: Gewerbestrasse 11, 6330 Cham, Switzerland

Foreword

I am excited and honored to write the foreword for the book *Hybrid PET/MR Neuroimaging: A Comprehensive Approach* edited by the father and daughter team, Dinko and Ana Franceschi (my trainee!). Dinko has 30 years' experience in nuclear medicine and has clearly recognized hybrid PET-MRI is an important new technology that will completely change our practice futures. I helped train Ana in neuroradiology and PET-MRI – in just a few years, Ana has become a recognized early expert and champion for using this technology in routine clinical practice, first in the New York City area, and now at national meetings for neuroradiology and nuclear medicine. Ana and Dinko have collaborated with established and emerging leaders in this new field to cover the expanding scope and impact of hybrid PET-MRI. My only complaint is that I actually needed this book in the summer of 2012! Now there will be an excellent resource for physicians with different training and clinical backgrounds who are interested in learning more about the utility and interpretation of hybrid PET-MRI for neurological diseases.

My own early personal experience with PET-MRI may be instructive to readers interested in getting started since NYU was one of the first programs to use PET-MRI for clinical practice – i.e. what it was like in the “old days” before this helpful book was available. I suspect many of the chapter authors can tell similar stories. When I arrived at NYU in August 2012 fresh out of fellowship, we had just installed a hybrid PET-MRI scanner in the main outpatient radiology facility. Yvonne Lui, my section chief, asked me to be the neuroradiology liaison for PET-MRI clinical and research studies. After neuroradiology fellowship training, I was quite familiar with the role of MRI in the clinical management of epilepsy and dementia, was an “authorized user,” and had decent trainee-level experience with FDG PET for cancer imaging (maybe 50 cases). My proudest accomplishment in nuclear medicine though may have been my autographed copy of Mettler's textbook obtained when he visited UCSF during boards preparation. At that point, I had read three FDG PET brain studies in my “career” – one of those was for the radiology board exam in a hotel room in Louisville in 2011 and to this day I think I failed that case! We were unsure how to apply this new technology, but started using a research protocol that allowed us to pay for a cab and transport patients after their routine FDG PET-CT at the NYU cancer center across midtown Manhattan to be reimaged on the PET-MRI scanner at the radiology outpatient facility on First Avenue using the original decaying FDG dose.

It began as a trickle of patients. Over the next 2 years, I learned on the job how to really analyze and interpret FDG PET from Kent Friedman, chief of NYU nuclear medicine. Kent and I reviewed the MRI and FDG PET images together once a week in a dual-readout format and prepared two separate reports. We were lucky not to have turf wars between sections and combined our expertise to interpret these studies. It was a time of discovery as we encountered real patients that forgot to read the textbooks before they showed up for imaging and we always had lots of questions – it was perhaps my limited knowledge of the FDG PET literature in the 1970–1980s that led me to “rediscover” key features for PET interpretation in epilepsy patients. After only seven patients had consented to both PET-CT and PET-MRI studies, the NYU level IV epilepsy center stopped ordering PET-CT for their patients and switched exclusively to PET-MRI studies. Eighteen months later in summer 2014, we opened the “floodgates”

and agreed to use this new technology to image patients with suspected cognitive impairment from the NYU Pearl Barlow memory and aging center. Our volume immediately doubled, then doubled again over the next 18 months. Today, we typically interpret 25–30 clinical neuroradiology PET-MRI studies a week (~1200 per year) – a volume dominated by cognitive impairment workup, but we also image patients weekly for epilepsy, autoimmune encephalitis, brain, and neck tumors. Last time I checked in 2016, overall brain PET FDG volume was up 300% from 2012. We were one of the few sites to contribute to the original IDEAS study with hybrid PET-MRI data using amyloid tracers and routinely use multiple additional radiotracers in clinical practice and research (e.g., Dotatate, Tau, and TSPO tracers). I would predict that the recent FDA approval of Aduhelm, the amyloid-lowering immunotherapy from Biogen, also may increase our volume substantially.

Hybrid PET-MRI has changed our practice and actually changed the way I interpret MRI even without simultaneous PET. Over time those subtle MRI calls on epilepsy studies I was wary of mentioning in a conference at a well-known level IV epilepsy center for fear of my life were corroborated by the simultaneously acquired FDG PET, then subsequent intracranial EEG and surgical pathology. It is quite humbling to realize that subtle hippocampal sclerosis you were so excited to detect was just the tip of the iceberg in epilepsy patients and many of those “icebergs” were not even detectable with state-of-the-art MRI sequences. Conversely, MRI findings redirected us to recognize subtle extra-temporal FDG abnormalities we missed on an initial review that correlated well with semiology, EEG, and eventually surgical pathology. NYU referrers became very reliant on the PET-MRI reads we provide. Next Monday at our weekly multidisciplinary conference all four epilepsy patients considering surgery will have had hybrid FDG PET-MRI first. We had a similar experience changing the workup for neurodegenerative disease – instead of equivocating on ambiguous FDG PET findings or using MRI only to assess white matter disease, mass, and hydrocephalus, we started providing constellations of multimodal imaging findings to support workup for specific diagnoses. Particularly for dementia, we observed a changing role for radiologists in the triage of patients. Busy general neurology referrers that may not have expertise or time on the initial visit to distinguish the causes for word-finding difficulty would change their follow-up evaluations and management based on our PET-MRI report. Conversely, experts in primary progressive aphasia would use such reports to focus their practice, time, and resources. In epilepsy, neurodegenerative disease, and autoimmune encephalitis, you learn quickly you cannot hide from the limits of sensitivity and specificity for MRI findings we proudly teach residents once you see the much more obvious findings on simultaneously acquired FDG PET. Previous groups had shown the advantages of reinterpreting separately acquired PET and MRI together in epilepsy and dementia respectively [1, 2] – we were just turning that into daily clinical practice with a single efficient imaging session that patients, referrers, and the interpreting radiologists clearly preferred. I expect this phenomenon to continue and to expand to other common neurologic diseases as the technology and radiochemistry develop.

The biggest challenge to this new paradigm is finding physicians comfortable reading these studies by themselves, but this also results in the most powerful diagnostic confidence and efficient workflow. Our rapidly increasing volume showed quite clearly that hybrid PET-MRI was addressing an unmet need for our referrers – I would come back from 2 weeks of relaxing summer vacation with 30–40 cases waiting for me! An individual reader needs to be knowledgeable in several diverse areas that Ana, Dinko, and their chapter authors have made sure are well-covered by this book – neuroanatomy, PET physics and artifacts, potential compromises in imaging physics associated with hybrid PET-MRI (e.g., attenuation correction), FDG and various common radiotracers, software visualization tools and limitations. In 2013–15, I’m not convinced anyone came out of training with that complete skillset. Faculty with dual fellowship training in nuclear medicine and neuroradiology were as common as unicorns with zebra stripes (that is now changing). Very few nuclear medicine fellowship training programs are exposing trainees to even 50 FDG PET brain studies per year. I feel there remains a strong need and responsibility to train more people, and this book will be a tremendous help to that process.

Every year the NYU fellowship program trains 6–7 fellows to read PET-MRI with each fellow reading more than 100 cases during the year. Some may argue the PET is a waste of time for “regular” neuroradiologists, but it teaches them humility regarding the limitations of MRI and makes them better readers. Often we would see something or a question would come up during read up that I did not have a good answer for or could easily find in the PET literature – this book offers an up-to-date comprehensive resource for those frequent situations! In a messianic tone, I always foretell to the fellows that behind the current noise of deep learning, PET-MRI will revolutionize our field and that if they plan to practice for more than 10 years they *will* be reading PET-MRI studies. Ana Franceschi was the fellow who actually listened to me!

With this excellent introductory and first book focused on hybrid PET-MRI in neuroimaging, the secret should be out. I can *finally* retire my lecture titled “PET-MRI will change neuroradiology practice” that I have given over the past 7 years on podcasts and at many US institutions, national, and international meetings. When reading the chapters of this book, I encourage readers to think about our collective future. We all may be anxious about “deep learning” where clinical diagnosis and management are replaced by inscrutable layered algorithms from Skynet based just on existing MRI protocols... yet all the deep learning in the world could not solve the longitude navigation problem in the 1700s without an accurate clock (i.e., the right data). PET tracers increase the dimensionality of imaging data and are already being used to complement big data approaches to clinical imaging challenges in neurological diseases. The underlying reality is that hybrid PET-MRI is already starting to transform imaging for patients with neurological disease. It is not hard to see areas where imaging can improve in 2021; the MS patient with stable-appearing MRI that no longer walks unassisted into their follow-up scan, the young adult patient with smoldering autoimmune encephalitis or TBI that everyone thinks is just depressed, or patients in the early stages of movement disorders with normal-appearing MRI. Research with hybrid PET-MRI in carefully characterized clinical patients should validate new biomarkers particularly with novel MRI contrasts and quantitative approaches. MRI also transforms PET with dose reduction and increased spatial resolution using joint reconstruction techniques. The development of new PET tracers will only accelerate this holistic and synergistic process between two dynamic imaging technologies. Ana and Dinko have picked the perfect time to create a book introducing us to this promising new technology. I hope you find this book helpful and exciting for the future of diagnostic neuroimaging.

New York, NY, USA
June 2021

Tim Shepherd
Associate Section Chief, NYU Neuroradiology

References

1. Salamon et al. FDG-PET/MRI co-registration improves detection of cortical dysplasia in patients with epilepsy. *Neurology*. 2008;71(20):1594-601.
2. Shaffer et al. Predicting cognitive decline in subjects at risk for Alzheimer’s disease by using combined cerebrospinal fluid, MR imaging, and PET biomarkers. *Radiology*. 2013;266(2):583-91.

Contents

Part I Introduction to PET/MRI

- 1 Physics of PET/MRI Systems** 3
Paul Vaska and Lemise Saleh
- 2 PET Radiopharmaceutical Development** 9
Peter M. Smith-Jones
- 3 Attenuation Correction and Quantitative PET Analysis** 17
Mario Serrano-Sosa, Ana M. Franceschi, and Chuan Huang
- 4 Motion Correction in PET/MRI** 27
Mario Serrano-Sosa and Chuan Huang
- 5 The Use of Dual Modality PET/MRI in Population Studies:
Considerations on Exposures, Economics, Strengths, and Limitations** 35
Minos Kritikos and Sean A. P. Clouston
- 6 Introduction to Molecular Neuroimaging Applications** 45
Elizabeth Tong and Ghiam Yamin
- 7 Advanced Neuroimaging for Prevention of Brain Aging** 57
Diana A. Hobbs and Cyrus A. Raji
- 8 AI for Decision Support in Molecular Neuroimaging** 67
Guido A. Davidzon and Henry Li
- 9 Future Trends of PET/MR and Utility of AI in Multi-Modal Imaging** 79
Sheng-Che Hung, Mingxia Liu, Pew-Thian Yap, Dinggang Shen, Weili Lin,
and Mauricio Castillo

Part II Radiotracers in Neurologic PET/MRI

- 10 [¹⁸F]-FDG PET/MR Neuroimaging: Focus on Neuro-Oncology
Applications** 89
Hossein Shooli, Majid Assadi, and Mariam Aboian
- 11 Amyloid Imaging in Dementia and Neurodegenerative Disease** 99
Maria Rosana Ponisio, Pooya Iranpour, and Tammie L. S. Benzinger
- 12 Tau Imaging in Neurodegenerative Dementia** 111
Maria Rosana Ponisio, Pooya Iranpour, and Tammie L. S. Benzinger
- 13 FDOPA in Movement Disorders and Neuro-Oncology** 121
Maria Rosana Ponisio, Pooya Iranpour, and Tammie L. S. Benzinger

14	Amino Acid PET/MRI in Neuro-oncology	137
	Hossein Shooli, Majid Assadi, S. Ali Nabavizadeh, and Mariam Aboian	
15	Radioligands for Serotonin Receptors and Transporter PET Imaging	167
	Diane J. Kim and Chuan Huang	
16	Radioligands for Imaging of the CNS Acetylcholinergic System	179
	Mark Slifstein and Anissa Abi-Dargham	
17	Microglial Activation and Neuroinflammation	191
	William Charles Kreisl	
18	¹⁵O PET Imaging: Methods and Applications	197
	Hongyu An, Manu S. Goyal, and William J. Powers	
19	[⁶⁸Ga]-DOTATATE PET in the Central Nervous System	217
	Michelle Roytman and Jana Ivanidze	
Part III Dementia and Neurodegenerative Disease		
20	Neurology Evaluation in Dementia and Neurodegenerative Disease	227
	Luca Giliberto	
21	Neuropsychology Assessment in Dementia and Neurodegenerative Disease	247
	Shawn Mordhorst, Kelly Coulehan, and Emily C. Roseman	
22	Alzheimer's Disease	257
	Michelle Roytman, Marc L. Gordon, and Ana M. Franceschi	
23	Cerebral Amyloid Angiopathy	273
	Nelly Joseph-Mathurin and Cyrus A. Raji	
24	Posterior Cortical Atrophy	283
	Michelle Roytman and Jana Ivanidze	
25	Dementia with Lewy Bodies	291
	Jennifer Pitman and Gloria C. Chiang	
26	Behavioral Variant Frontotemporal Dementia	303
	Jeremy Ford and Gloria C. Chiang	
27	Logopenic Variant Primary Progressive Aphasia	313
	Michelle Roytman and Gloria C. Chiang	
28	Semantic Variant Primary Progressive Aphasia	323
	Marc L. Gordon and Ana M. Franceschi	
29	Nonfluent-Agrammatic Variant Primary Progressive Aphasia	337
	Michelle Roytman, Marc L. Gordon, and Ana M. Franceschi	
30	Progressive Supranuclear Palsy	347
	Jennifer Pitman and Jana Ivanidze	
31	Multiple System Atrophy	361
	Carlos Zamora, Mitchel A. Muhleman, and Mauricio Castillo	
32	Corticobasal Degeneration	373
	Martin Niethammer	

33 Creutzfeldt-Jakob Disease	387
Ilhami Kovanlikaya and Gloria C. Chiang	
34 Amyotrophic Lateral Sclerosis	397
Andrew D. Schweitzer and A. John Tsiouris	
35 Huntington's Disease	411
Carlos Zamora, Mitchel A. Muhleman, and Mauricio Castillo	
36 Parkinson's Disease	421
Martin Niethammer and Ana M. Franceschi	
37 Vascular Cognitive Impairment	441
Anand V. Patel and Richard B. Libman	
38 Normal Pressure Hydrocephalus	459
Ilhami Kovanlikaya and Gloria C. Chiang	
39 Crossed Cerebellar Diaschisis	469
Michael Clifton, Kiyon Naser-Tavakolian, and Ana M. Franceschi	
40 Traumatic Brain Injury and Chronic Traumatic Encephalopathy	479
Mateus Rozalem Aranha, Artur Martins Coutinho, Claudia da Costa Leite, and Carlos Alberto Buchpiguel	
 Part IV Epilepsy	
41 Epilepsy Localization: Introduction	495
Andrew Chiu and Michael Zeineh	
42 Developmental Disorders and Pediatric Epilepsy	499
Andrew Chiu and Michael Zeineh	
43 Acquired Pathology	507
Andrew Chiu and Michael Zeineh	
44 Treatment Planning	519
Andrew Chiu and Michael Zeineh	
45 Future Trends in Epilepsy Imaging	523
Andrew Chiu and Michael Zeineh	
 Part V Neuro-Oncology	
46 Neuro-Oncology: Imaging Diagnosis	527
Otto Rapalino	
47 Primary Brain Neoplasms	539
Salma O. Abbas, Sohil H. Patel, and Sugoto Mukherjee	
48 Intracranial Metastatic Disease	565
David Joyner and Jeffrey Hooker	
49 Treatment Planning	579
Otto Rapalino	
50 Treatment Response	589
Tuba Kalelioglu and Sohil H. Patel	

Part VI CNS Inflammatory and Infectious Disease

- 51 Infectious Disease**599
Sanaz Ghaderi Niri, Prashant Raghavan, and Max Wintermark
- 52 Inflammatory Disease**611
Sanaz Ghaderi Niri, Prashant Raghavan, and Max Wintermark
- 53 Demyelinating Disease**617
Sanaz Ghaderi Niri, Prashant Raghavan, and Max Wintermark
- 54 Vasculitis**621
Sanaz Ghaderi Niri, Prashant Raghavan, and Max Wintermark

Part VII Hybrid Imaging in Head and Neck

- 55 Role of PET/MR in Squamous Cell Cancer Staging**627
Gagandeep Choudhary and Houman Sotoudeh
- 56 Squamous Cell Cancer: Mucosal, Nodal and Extranodal Disease**639
Claudia F. E. Kirsch
- 57 Metastatic Disease in the Head and Neck**657
Houman Sotoudeh and Gagandeep Choudhary
- 58 Orbital Pathology**671
Vikas Jain, Osama Ahmed, and Ana M. Franceschi
- 59 Salivary Gland Pathology**689
Vikas Jain, Osama Ahmed, Mohit Agarwal, and Ana M. Franceschi

Part VIII Spine PET/MRI

- 60 Spinal Neoplasms**713
Jolie Jean and Jana Ivanidze
- 61 Non-Neoplastic Spinal Pathologies**723
Jolie Jean, David J. Hastie, and Jana Ivanidze

Part IX Pediatric PET/MRI Neuroimaging

- 62 Pediatric PET/MRI Neuroimaging: Overview**737
Christian Pedersen, Steven Messina, Heike Daldrup-Link, and Mariam Aboian
- 63 Pediatric Epilepsy: Non-oncologic Applications of PET/MRI**741
Steven Messina, Christian Pedersen, Heike Daldrup-Link, and Mariam Aboian
- 64 Pediatric Brain and Head-Neck Oncology**753
Christian Pedersen, Steven Messina, Heike Daldrup-Link, and Mariam Aboian
- 65 Pediatric Spine**765
Christian Pedersen, Heike-Daldrup Link, and Mariam Aboian

Part X Vascular Hybrid Imaging

66 Cerebral Small Vessel Disease	781
Bhanu Gogia, Richard B. Libman, and Anand V. Patel	
67 Aneurysms and Vascular Malformations	793
Tanvir Rizvi	
68 Genetic Stroke Syndromes	805
Anand V. Patel, Chilvana V. Patel, and Richard B. Libman	
69 Perfusion PET and Cerebrovascular Reactivity with Acetazolamide Versus CO₂ Challenge	827
Farshad Moradi and Audrey P. Fan	
70 Advanced MR Perfusion Techniques	839
Jeffers Nguyen and Jana Ivanidze	
71 Imaging of Glymphatic Flow and Neurodegeneration	849
Christopher G. Filippi and Richard Watts	
Index	861

Contributors

Salma O. Abbas Department of Radiology and Medical Imaging, University of Virginia Health System, Charlottesville, VA, USA

Anissa Abi-Dargham Department of Psychiatry and Behavioral Health, Renaissance School of Medicine, Stony Brook University, Stony Brook, NY, USA

Mariam Aboian Yale University School of Medicine, New Haven, CT, USA
Section of Neuroradiology and Nuclear Medicine, Yale School of Medicine, New Haven, CT, USA

Mohit Agarwal Department of Radiology, Medical College of Wisconsin, Milwaukee, WI, USA

Osama Ahmed Department of Radiology, Stony Brook University Hospital, Stony Brook, NY, USA

Hongyu An Mallinckrodt Institute of Radiology, Washington University School of Medicine in St. Louis, St. Louis, MO, USA

Mateus Rozalem Aranha Laboratory of Magnetic Resonance in Neuroradiology (LIM 44), Institute of Radiology, Hospital das Clínicas, Faculdade de Medicina da Universidade de São Paulo (HC-FMUSP), São Paulo, SP, Brazil

Laboratory of Nuclear Medicine (LIM 43), Center of Nuclear Medicine, Institute of Radiology, Hospital das Clínicas, Faculdade de Medicina da Universidade de São Paulo (HC-FMUSP), São Paulo, SP, Brazil

Majid Assadi The Persian Gulf Nuclear Medicine Research Center, Department of Molecular Imaging and Radionuclide Therapy (MIRT), Bushehr Medical University Hospital, Faculty of Medicine, Bushehr University of Medical Sciences, Bushehr, Iran

Tammie L. S. Benzinger Mallinckrodt Institute of Radiology, Washington University School of Medicine in St. Louis, St. Louis, MO, USA

Carlos Alberto Buchpiguel Laboratory of Nuclear Medicine (LIM 43), Center of Nuclear Medicine, Institute of Radiology, Hospital das Clínicas, Faculdade de Medicina da Universidade de São Paulo (HC-FMUSP), São Paulo, SP, Brazil

Mauricio Castillo Division of Neuroradiology, Department of Radiology, University of North Carolina School of Medicine, Chapel Hill, NC, USA

Gloria C. Chiang Department of Radiology, New York Presbyterian-Weill Cornell Medicine, New York, NY, USA

New York Presbyterian-Weill Cornell, Department of Radiology, New York, NY, USA

Andrew Chiu Stanford University, Department of Radiology, Stanford, CA, USA

Gagandeep Choudhary Department of Radiology, University of Alabama at Birmingham (UAB), Birmingham, AL, USA

Michael Clifton, MD Department of Radiology, Stony Brook Renaissance School of Medicine/University Hospital, Stony Brook, NY, USA

Sean A. P. Clouston Renaissance School of Medicine, Stony Brook University, Stony Brook, NY, USA

Artur Martins Coutinho Laboratory of Nuclear Medicine (LIM 43), Center of Nuclear Medicine, Institute of Radiology, Hospital das Clínicas, Faculdade de Medicina da Universidade de São Paulo (HC-FMUSP), São Paulo, SP, Brazil

Claudia da Costa Leite Laboratory of Magnetic Resonance in Neuroradiology (LIM 44), Institute of Radiology, Hospital das Clínicas, Faculdade de Medicina da Universidade de São Paulo (HC-FMUSP), São Paulo, SP, Brazil

Renaissance School of Medicine at Stony Brook University, Health Sciences Center, Level 4, Stony Brook, NY, USA

Heike Daldrup-Link Department of Radiology and Molecular Imaging Program at Stanford (MIPS), Stanford School of Medicine, Stanford, CA, USA

Guido A. Davidzon Division of Nuclear Medicine & Molecular Imaging, Department of Radiology, Stanford University, Stanford, CA, USA

Audrey P. Fan Department of Neurology, University of California, Davis, CA, USA

Christopher G. Filippi Department of Radiology, Tufts Medical Center, Tufts University School of Medicine, Boston, MA, USA

Jeremy Ford New York Presbyterian-Weill Cornell, Department of Radiology, New York, NY, USA

Ana M. Franceschi Donald and Barbara Zucker School of Medicine at Hofstra/Northwell, The Feinstein Institutes for Medical Research, Manhasset, NY, USA

Division of Neuroradiology, Department of Radiology, Lenox Hill Hospital, Northwell Health, New York, NY, USA

Dinko Franceschi Division of Nuclear Medicine, Department of Radiology, Stony Brook University Hospital, Renaissance School of Medicine at Stony Brook University, Stony Brook, NY, USA

Luca Giliberto Litwin-Zucker Center for the Study of Alzheimer's Disease and Memory Disorders, Feinstein Institutes for Medical Research and Institute for Neurology and Neurosurgery, Northwell Health System, Manhasset, NY, USA

Bhanu Gogia Department of Neurology, University of Texas Medical Branch, Galveston, TX, USA

Marc L. Gordon Zucker Hillside Hospital, Donald and Barbara Zucker School of Medicine at Northwell/Hofstra, The Litwin-Zucker Research Center, The Feinstein Institutes for Medical Research, Manhasset, NY, USA

Manu S. Goyal Mallinckrodt Institute of Radiology, Washington University School of Medicine in St. Louis, St. Louis, MO, USA

David J. Hastie Tufts University School of Medicine, Boston, MA, USA

Diana A. Hobbs Department of Radiology, Washington University School of Medicine, St. Louis, MO, USA

Jeffrey Hooker Department of Radiology and Medical Imaging, University of Virginia Health System, Charlottesville, VA, USA

Chuan Huang Department of Psychiatry and Behavioral Health, Renaissance School of Medicine at Stony Brook University, Stony Brook, NY, USA

Department of Radiology, Renaissance School of Medicine at Stony Brook University, Stony Brook, NY, USA

Sheng-Che Hung Division of Neuroradiology, Department of Radiology, University of North Carolina School of Medicine, Chapel Hill, NC, USA

Biomedical Research Imaging Center, University of North Carolina, Chapel Hill, NC, USA

Pooya Iranpour Richard L. Roudebush VA Medical Center, Department of Nuclear Medicine, Indianapolis, IN, USA

Jana Ivanidze, MD, PhD Department of Diagnostic Radiology, Division of Molecular Imaging and Therapeutics, Division of Neuroradiology, Molecular Imaging Innovations Institute, Weill Cornell Medicine, Department of Radiology, New York, NY, USA

Vikas Jain MetroHealth Medical Center, Case Western Reserve University, Cleveland, OH, USA

Jolie Jean Tufts University School of Medicine, Boston, MA, USA

Nelly Joseph-Mathurin Mallinckrodt Institute of Radiology, Washington University School of Medicine, Saint Louis, MO, USA

David Joyner Department of Radiology and Medical Imaging, University of Virginia Health System, Charlottesville, VA, USA

Tuba Kalelioglu Department of Radiology and Medical Imaging, UVA Health System, Charlottesville, VA, USA

Diane J. Kim Department of Psychiatry and Behavioral Health, Renaissance School of Medicine at Stony Brook University, Stony Brook, NY, USA

Claudia F. E. Kirsch Department of Radiology Northwell Health, Zucker Hofstra School of Medicine at Northwell, North Shore University Hospital, Manhasset, NY, USA

Ilhami Kovanlikaya New York Presbyterian-Weill Cornell, Department of Radiology, New York, NY, USA

William Charles Kreisl The Taub Institute for Research on Alzheimer's Disease and the Aging Brain, Columbia University Irving Medical Center, New York, NY, USA

Minos Kritikos Renaissance School of Medicine, Stony Brook University, Stony Brook, NY, USA

Richard B. Libman Neurology, Vascular Neurology, Northwell Health Physician Partners Neuroscience Institute at Great Neck, Great Neck, NY, USA

Henry Li Department of Radiology, Stanford University, Stanford, CA, USA

Heike-Daldrup Link Department of Radiology and Molecular Imaging Program at Stanford (MIPS), Stanford School of Medicine, Stanford, CA, USA

Weili Lin Division of Neuroradiology, Department of Radiology, University of North Carolina School of Medicine, Chapel Hill, NC, USA

Biomedical Research Imaging Center, University of North Carolina, Chapel Hill, NC, USA

Mingxia Liu Biomedical Research Imaging Center, University of North Carolina, Chapel Hill, NC, USA

Department of Radiology, University of North Carolina, Chapel Hill, NC, USA

Steven Messina Radiology (Division of Neuroradiology), Mayo Clinic, Rochester, MN, USA

Farshad Moradi Division of Nuclear Medicine, Department of Radiology, Stanford University, Stanford, CA, USA

Shawn Mordhorst Renaissance School of Medicine at Stony Brook University, Health Sciences Center, Level 4, Stony Brook, NY, USA

Mitchel A. Muhleman Division of Molecular Imaging and Therapeutics, Department of Radiology, University of North Carolina School of Medicine, Chapel Hill, NC, USA

Sugoto Mukherjee Department of Radiology and Medical Imaging, University of Virginia Health System, Charlottesville, VA, USA

S. Ali Nabavizadeh University of Pennsylvania/Perelman School of Medicine, Philadelphia, PA, USA

Kiyon Naser-Tavakolian Department of Radiology, Stony Brook Renaissance School of Medicine/University Hospital, Stony Brook, NY, USA

Jeffers Nguyen Donald and Barbara Zucker School of Medicine at Hofstra/Northwell, Department of Radiology, Hempstead, NY, USA

Martin Niethammer Center for Neurosciences, The Feinstein Institutes for Medical Research, Manhasset, NY, USA

Department of Neurology, North Shore University Hospital, Manhasset, NY, USA

Sanaz Ghaderi Niri Division of Neuroradiology, Johns Hopkins University, Baltimore, MD, USA

Anand V. Patel Department of Radiology and Medical Imaging, University of Virginia Health System, Charlottesville, VA, USA

Chilvana V. Patel Department of Neurology, Neurophysiology Fellowship Training Program University of Texas Medical Branch, Galveston, TX, USA

Sohil H. Patel Department of Radiology and Medical Imaging, UVAH Healthsystem, Charlottesville, VA, USA

Christian Pedersen Mercy Catholic Medical Center, Trinity Health Mid-Atlantic, Department of Radiology, Darby, PA, USA

Jenifer Pitman, MD New York Presbyterian-Weill Cornell, Department of Radiology, New York, NY, USA

Division of Neuroradiology, Weill Cornell Medicine, Department of Radiology, New York, NY, USA

Bruno Policeni University of Iowa Hospitals and Clinics, Iowa City, IA, USA

Maria Rosana Ponisio Mallinckrodt Institute of Radiology, Washington University School of Medicine in St. Louis, St. Louis, MO, USA

William J. Powers Department of Neurology, University of North Carolina School at Chapel Hill, Chapel Hill, NC, USA

Prashant Raghavan Division of Neuroradiology, Department of Diagnostic Radiology and Nuclear Medicine, University of Maryland School of Medicine, Baltimore, MD, USA

Cyrus A. Raji Mallinckrodt Institute of Radiology, Washington University School of Medicine, Saint Louis, MO, USA

Mallinckrodt Institute of Radiology, Department of Radiology, Saint Louis, MO, USA

Otto Rapalino Harvard Medical School, Boston, MA, USA

Massachusetts General Hospital, Boston, MA, USA

Tanvir Rizvi Department of Radiology and Medical Imaging, University of Virginia Health System, Charlottesville, VA, USA

Emily C. Roseman Renaissance School of Medicine at Stony Brook University, Health Sciences Center, Level 4, Stony Brook, NY, USA

Michelle Roytman, MD Department of Radiology, NewYork-Presbyterian Hospital/Weill Cornell Medicine, New York, NY, USA

Lemise Saleh Department of Biomedical Engineering, Stony Brook University, Stony Brook, NY, USA

Pina C. Sanelli Institute of Health Innovations and outcomes Research, Feinstein Institutes for Medical Research, Manhasset, NY, USA

Andrew D. Schweitzer Department of Radiology, NewYork-Presbyterian Hospital - Weill Cornell Medicine, New York, NY, USA

Dinggang Shen School of Biomedical Engineering, ShanghaiTech University, Shanghai, China

Department of Research and Development, Shanghai United Imaging Intelligence Co., Ltd., Shanghai, China

Hossein Shooli The Persian Gulf Nuclear Medicine Research Center, Department of Molecular Imaging and Radionuclide Therapy (MIRT), Bushehr Medical University Hospital, Faculty of Medicine, Bushehr University of Medical Sciences, Bushehr, Iran

Mark Slifstein Department of Psychiatry and Behavioral Health, Renaissance School of Medicine, Stony Brook University,, Stony Brook, NY, USA

Peter M. Smith-Jones Department of Radiology, Stony Brook University Hospital, Stony Brook, NY, USA

Mario Serrano-Sosa Department of Radiology, Stony Brook Medicine, Stony Brook, NY, USA

Houman Sotoudeh Department of Radiology, University of Alabama at Birmingham (UAB), Birmingham, AL, USA

Elizabeth Tong Stanford Health Care, Department of Neuroimaging & Neurointervention, Stanford, CA, USA

A. John Tsiouris Department of Radiology, NewYork-Presbyterian Hospital - Weill Cornell Medicine, New York, NY, USA

Paul Vaska Departments of Biomedical Engineering and Radiology, Renaissance School of Medicine at Stony Brook University, Stony Brook, NY, USA

Richard Watts Brain Imaging Center, Department of Psychology, Yale University, New Haven, CT, USA

Max Wintermark Department of Rad/Neuroimaging and Neurointervention, Stanford Medical Center, Stanford, CA, USA

Ghiam Yamin Stanford Health Care, Department of Neuroimaging & Neurointervention, Stanford, CA, USA

Pew-Thian Yap Biomedical Research Imaging Center, University of North Carolina, Chapel Hill, NC, USA

Department of Radiology, University of North Carolina, Chapel Hill, NC, USA

Carlos Zamora Division of Neuroradiology, Department of Radiology, University of North Carolina School of Medicine, Chapel Hill, NC, USA

Michael Zeineh Stanford University, Department of Radiology, Stanford, CA, USA

Part I

Introduction to PET/MRI

Dinko Franceschi



Future Trends of PET/MR and Utility of AI in Multi-Modal Imaging

9

Sheng-Che Hung, **Mingxia Liu**, Pew-Thian Yap, Dinggang Shen, Weili Lin, and Mauricio Castillo

Recent Advances and Future Trends of PET/ MR

Hardware

Over the past decade, hardware advances, including lutetium-based scintillators, solid-state-based silicon photomultiplier (SiPM)-based detectors, time-of-flight (TOF) imaging, improved detector design, and 3D PET, contributed to improved PET quality [1]. One of the most recent trends is the total-body PET (TB-PET). Standard axial field of view (FOV) in commercial PET scanners ranges from 15 to 26 cm and requires multiple bed translation to acquire a whole-body scan. The idea of TB-PET is to extend the axial FOV to cover the whole body with an increased number of detectors [2]. There are currently two NIH-funded TB-PET systems for human use: the PennPET Explorer (axial FOV, 140 cm) developed by the University of Pennsylvania/KAGE medical team and Philips in 2018, and the uExplorer (axial FOV, 194 cm) developed by the UC Davis/United Imaging team in 2019. Advantages of these TB-PET design are twofold:

1. Whole-body imaging can be acquired in a one-bed position in the same time frame.

2. Detection efficiency is improved by collecting photon pairs emitted from organs that would be originally outside the FOV or the photons emitted from organs inside the FOV but that do not intercept the detector ring.

Overall, TB-PET can contribute to a >40-fold increase in effective sensitivity and a >6-fold increase in SNR compared with current whole-body PET [2]. The large gain of higher detection efficiency can be utilized to optimize scan parameters to achieve different goals, including:

1. Improving imaging quality by controlling the same acquisition time and administered dose
2. Reducing radiotracer dose according to the degree of sensitivity increase by controlling the same acquisition time and the same diagnostic image quality
3. Shortening scan time by maintaining the same radioactive dose and the same image quality

Potential benefits of TB-PET have been elaborated in several reviews [3, 4]. In brief, increased PET sensitivity allows for detection of “lower-density” disease, such as cancer micrometastases, inflammation, or infection. It also allows for imaging of short-lived radiotracers at lower radioactivity or delayed PET to contrast the differential radiotracer uptake in various tissues. The low-dose protocol can significantly reduce radiation dose of each scan and allows for repeated scans for longitudinal and interventional research studies and widens indications to include non-oncological diseases such as imaging of bacterial infections, drug addiction, and neuroinflammation [5–7]. Low-dose PET is also useful in vulnerable populations such as children and pregnant women. Shorter scan times reduce motion artifacts in pediatric or restless patients, reduce patient discomfort, and improve patient throughput [2]. Furthermore, shorter scan times allow for faster dynamic scanning which can be used to monitor radiopharmaceutical pharmacokinetic distribution across multiple organs and systems. Although TB-PET design is currently only combined with CT and the cost of

S.-C. Hung (✉) · **M. Liu** (✉) · P.-T. Yap · W. Lin
Department of Radiology, University of North Carolina,
Chapel Hill, NC, USA

Biomedical Research Imaging Center, University of North
Carolina, Chapel Hill, NC, USA
e-mail: shengche_hung@med.unc.edu; mingxia_liu@med.unc.edu

D. Shen
School of Biomedical Engineering, ShanghaiTech University,
Shanghai, China

Department of Research and Development, Shanghai United
Imaging Intelligence Co., Ltd., Shanghai, China

M. Castillo
Department of Research and Development, Shanghai United
Imaging Intelligence Co., Ltd., Shanghai, China

total-body PET/MR would be high, the benefits of extending axial FOV in PET/MR will open new windows for research and clinical opportunities.

Imaging Reconstruction

Ordered subset expectation maximization (OSEM) is the most commonly used algorithm to generate the PET images by iterative reconstruction. The OSEM reconstruction methods improve image sharpness with a number of iterations at the expense of reducing signal-to-noise ratio, however. Thus, image reconstruction generally stops after a small number of iterations, and this results in an under-converged image. Technical advances, such as TOF imaging and 3D PET, can reduce noise and allow for a higher number of iterations to achieve higher imaging sharpness at comparable noise levels [8]. Recently, General Electric (GE) introduced a new reconstruction algorithm called “Bayesian Penalized Likelihood Image Reconstruction” that achieves a fully convergent iterative reconstruction and can significantly improve image SNR and accurate quantification compared to OSEM [9].

Quantitative Accuracy

MR-based AC is an important issue because MR images cannot provide metrics that can be converted to attenuation coefficient maps at 511 KeV. Originally, commercial PET/MR scanners generated the attenuation coefficient maps by a 3D “Dixon-VIBE” or “LAVA-FLEX” sequence to classify tissue into four classes (air, fat, lung, and soft tissue) [10]. The main limitation of these methods is that none of the classes truly correspond to bone. Erroneous misclassification of the bone as soft tissue in segmentation can cause spatially biased PET measurements. One of the latest approaches is the atlas-based method, which first derives an atlas based on a population database of CT/MR image pairs and then aligns the atlas to the target patient to synthesize pseudo-CT for AC. Atlas-based methods are proven robust and provide accurate results of brain PET AC [11]. However, these methods may cause a small but significant underestimation of uptake in the temporal lobes or regions near the skull base and cannot be used in patients with anatomic variations [12]. Another approach is direct imaging with ultrashort echo time (UTE) or zero echo time (ZTE). The UTE and ZTE sequences can generate signals in materials with short $T2^*$ such as cortical bone and then use this information for bone segmentation in the skull to synthesize pseudo-CT images. This direct imaging approach can overcome the inter-subject anatomic variations and may be applied to regions outside the brain [13]. Several studies have shown similar accuracy of PET measurements between ZTE-based and atlas-based AC maps [14]. However,

direct imaging methods are not as robust as atlas-based methods and can be negatively impacted by noise and image artifacts.

Furthermore, in addition to the bones, there are also extrinsic sources of biased AC in the scan, including pads used to keep the patient’s head still during the examination, dense hair, and headphones. One study showed that the bias of measurements by the pads is small (<3.1%), but that dense hair and headphones significantly bias the quantification (>10%). Although these issues are not discussed in the current commercial AC methods, it will be important to minimize these quantification biases for quantitative or longitudinal studies [15].

Motion Correction

Longer scan time makes PET/MR prone to motion when compared to PET/CT. A review of motion corrections focusing on PET or MR images alone is beyond the scope of this chapter. Here, we will focus on methods that have been investigated in PET/MR. To correct the motion-induced errors, there are several methods to measure subjects’ motion, namely, data-driven and marker tracking methods, respectively. The former approaches use acquired MR images, whereas the latter approaches may require add-on motion tracking systems to obtain motion information [16]. Brain COMPASS™ (Siemens Healthcare GmbH) is a data-driven method, which performs MR-based motion corrections based on a simultaneous acquisition of fast 3D echoplanar images during the scan. This method uses spatially and temporally aligned MR images as references for motion correction of PET [17]. One advantage of data-driven motion correction methods is that no additional hardware is needed. Its disadvantage is that the simultaneous acquisitions during PET prevent the MR unit from scanning other sequences, meaning that the MR-based PET motion correction increases the scan time. Also, the sampling frequency of MR images is limited by the acquisition time and is inferior to that of external tracking systems.

Marker tracking systems require additional optical, radioactive, or MR active fiducial markers temporarily attached to the subject’s head [18]. These systems are usually easy to set up but can only track external motions and bring up additional issues, such as patient discomfort, additional patient contact, or fiducial displacement. There are some markerless tracking methods. For example, a commercial system (Tracoline 2.0) can continuously extract the patient’s facial features with a synchronized light modulator and a camera outside the scanner [19]. The advantages of this marker-free tracking system include the unnecessary need for fiducials, reduction of the clinical preparation times compared to marker-based methods, and elimination of the possibility of

tracking failure due to marker displacement. However, this system requires additional cross-calibration between the tracking coordinate system and the device coordinate system before each scan and prolongs scan time. Another marker-free tracking system takes advantage of in-bore stereo-optical sensors (HobbitView Inc.) which are directly mounted to the head coil to capture the naive natural or amplified features on the forehead. This approach has been reported to be able to provide sub-millimeter and sub-degree accuracy in phantoms and volunteers [20]. However, the tracking markers of this approach are skin features of the forehead, which may be affected by facial movements, leading to erroneous pose estimation. Besides, the influence of the in-bore cameras on the attenuation maps requires further investigation.

Artificial Intelligence

AI is a rapid-growing field and has already widely impacted various, if not all, fields of PET/MR [21]. For example, deep learning can synthesize a “pseudo-CT” from MR images, or even ^{18}F -FDG non-attenuation corrected images alone can be used for AC [22]. Combining Dixon and ZTE to generate AC maps by the neural network is superior to the approaches based on Dixon images alone or based on the vendor-supplied ZTE segmentation [22]. It is also feasible, by using convolutional neural networks and generative adversarial networks, to denoise PET images and reduce the radiotracer dose to 25% of the standard dose and lower by estimating standard-dose PET images from the low-dose PET images and inputs of multiparametric MRI [23–26].

Utility of AI in Multi-Modal Imaging

MRI and PET have been widely used for the diagnosis of Alzheimer’s disease (AD) and conversion prediction of mild cognitive impairment (MCI). A common challenge in multi-modal studies is the missing data problem [27, 28]. In clinical practice, subjects who are willing to be scanned by MRI may reject PET scans due to their high cost and other issues such as concern of radioactive exposure. In the baseline, Alzheimer’s Disease Neuroimaging Initiative (ADNI-1) [29], only approximately one-half of subjects have PET scans, although all subjects have MRI data. Previous studies usually tackle this problem by simply discarding subjects without PET scans [30]. However, such a simple approach significantly reduces the number of training subjects for learning a reliable model, thus inevitably degrading diagnostic performance. Another commonly used strategy is to input the missing data/features of a subject using the mean or median feature values of other subjects (with complete data)

or even using random values [31], which brings additional noise and is only feasible for handcrafted features. To utilize all available subjects, an intuitive strategy is to impute the missing PET scans directly [32].

In multi-modal neuroimaging-based studies, one usually has a limited number (e.g., tens or hundreds) of training subjects which severely limits the generalization capacity of deep learning models [33, 34]. A commonly used strategy is to include disease-related prior knowledge to guide the extraction of feature representations from neuroimages. For example, prior biological/anatomical knowledge on dementia-associated brain changes/abnormalities has been used to identify local image patches for representing each image. Recently proposed deep learning methods aim to learn task-oriented features of neuroimages based on anatomical landmarks [30, 35]. These methods first define disease-related anatomical landmarks and then automatically extract features based on image patches (located by landmarks) avoiding using non-informative voxels and regions in the brain. Since these methods highly rely on expert knowledge on specific brain diseases, their general performance may be limited in practical applications.

Several advanced AI techniques via deep neural networks have been recently developed for automated brain disorder identification based on incomplete MRI and PET data. Below, we first discuss the problem formulation of neuroimaging-based disease diagnosis based on incomplete MRI and PET scans and then briefly address two recent studies on the topic.

Problem Formulation

It would be desirable to construct a computer-aided diagnosis system based on multi-modality data, such as MRI (denoted as \mathcal{A}) and PET (denoted as \mathcal{B}). Denote $\mathbf{M} = \{(\mathbf{A}_i, \mathbf{B}_i, y_i)\}_{i=1}^N$ as a dataset consisting of N subjects, where $\mathbf{A}_i \in \mathcal{A}$ and $\mathbf{B}_i \in \mathcal{B}$ denote the representations of MRI and PET for the i -th subject, respectively. Also, $y_i \in \{0, 1\}$ denotes the class label of the i -th subject, e.g., 1 for AD and 0 for healthy control (HC). In practice, not all subjects have complete data of both modalities.

As shown in Fig. 9.1, a general computer-aided disease diagnosis model F using complete multi-modal data can be formulated as

$$\hat{y}_i = F(\mathbf{A}_i, \mathbf{B}_i), \quad (9.1)$$

where \hat{y}_i is the estimated label for the i -th subject. Let $\hat{\mathbf{B}}_i = G(\mathbf{A}_i)$ denote data imputation with the mapping function G . Thus, the diagnosis model with complete (after PET synthesis) multi-modal data can be executed as

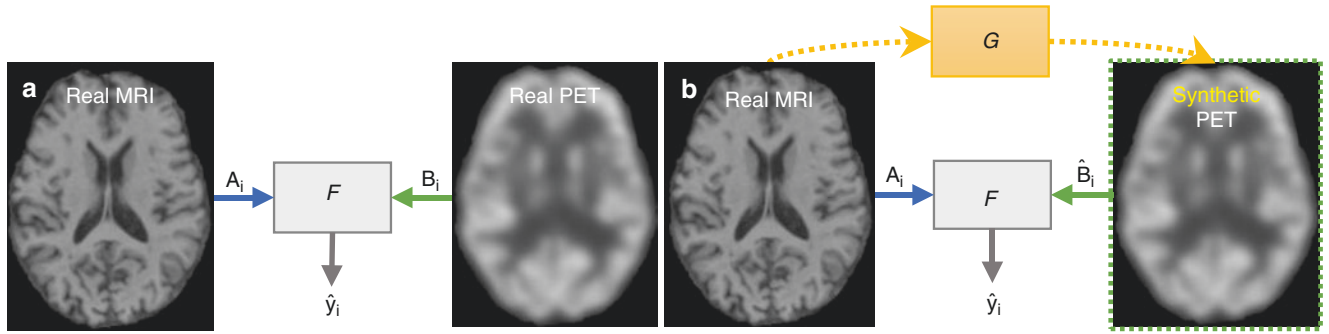


Fig. 9.1 (a) A diagnosis model F trained on the complete MRI and PET scans. (b) A diagnosis model F trained on the complete (after imputation for missing PET scans) data. A_i and B_i represent the MRI

and PET scans for the i -th subject, respectively. $\hat{B}_i = G(A_i)$ represents the synthesized PET scan via image generator G , and \hat{y}_i is the estimated label for the i -th subject

$$\hat{y}_i = F(A_i, B_i) \approx F \quad (9.3)$$

In the following sections, two AI approaches to synthesize missing PET images for subjects with only MR images will be first discussed, followed by a unified approach capable of imputing missing data and achieving clinical diagnosis.

Hybrid Cycle-Consistent GAN for Synthesizing PET/MRI

Cycle-consistent generative adversarial network (CGAN) [32] has been successfully applied to learning the bi-directional mappings between relevant image domains. Since MR and PET images scanned from the same subject have underlying relevance, Pan et al. [36, 37] resorted to a 3D CGAN model, called hybrid GAN (HGAN), to learn bi-directional mappings between MRI and PET through which a missing PET scan can be synthesized based on its corresponding MRI scan. Specifically, a two-stage deep learning framework was developed [36, 37] to employ all available MRI and PET for brain disease diagnosis. In the first stage, the missing PET images were imputed by bi-directional mappings between MRI and PET via HGAN. In the second stage, based on the complete MRI and PET (i.e., after imputation), a landmark-based multi-modal multi-instance learning method (LDMIL) [30] was used for AD diagnosis, by learning MRI and PET features automatically in a data-driven manner.

The architecture of the HGAN model is illustrated in Fig. 9.2, which consists of two generators (G_1 and G_2) and two adversarial discriminators (D_1 and D_2). As shown in Fig. 9.2, based on the underlying relevance between MRI and PET, a mapping function from MRI to PET is learned in HGAN, i.e., $G_1 : \mathcal{A} \rightarrow \mathcal{B}$. A reversed function $G_2 : \mathcal{B} \rightarrow \mathcal{A}$ is also learned to encourage G to be a one-to-one mapping, with the constraint of $G_2 = G_1^{-1}$. The adversarial discriminators (e.g., D_1)

are used to tell us whether the synthetic MR and corresponding real MR images are distinguishable or not. A cycle-consistent loss is used to learn the bi-directional mapping between MRI and PET aiming to guarantee the interactive relationship between the two modalities. More details on the network architecture and objective function of HGAN can be found elsewhere [36, 37].

Two subsets of the ADNI database [29], i.e., ADNI-1 and ADNI-2, were used for performance evaluation [36, 37]. There were 821 subjects in ADNI-1 and 636 subjects in ADNI-2. While all subjects in ADNI-1 and ADNI-2 had baseline MRIs, only 395 subjects in ADNI-1 and 254 subjects in ADNI-2 had PET images. All MR images were pre-processed via four steps: (1) anterior commissure (AC)-posterior commissure (PC) alignment, (2) skull stripping, (3) intensity correction, and (4) linear alignment to a template MRI. Each PET image was also aligned to its corresponding MRI via linear registration.

To evaluate the quality of the synthetic images, HGAN was first trained on the complete subjects (i.e., containing both PET and MRI scans) in ADNI-1 and then tested on the complete subjects in ADNI-2. Two typical subjects with real and synthetic PET scans are shown in Fig. 9.3. From Fig. 9.3, one can observe that the synthetic PET/MRI looks very similar to their corresponding real images. For instance, the mean and standard deviation of peak signal-to-noise ratio (PSNR) values of synthetic PET images in ADNI-2 are 24.49 ± 3.46 . These results imply that the HGAN model is reasonable, and that the synthetic PET scans have acceptable image quality (in terms of PSNR).

Disease-Image-Specific GAN for Joint Image Synthesis and Disease Diagnosis

The HGAN model in [36] equally treats all voxels in each 3D volume, thus ignoring the *disease-image specificity*

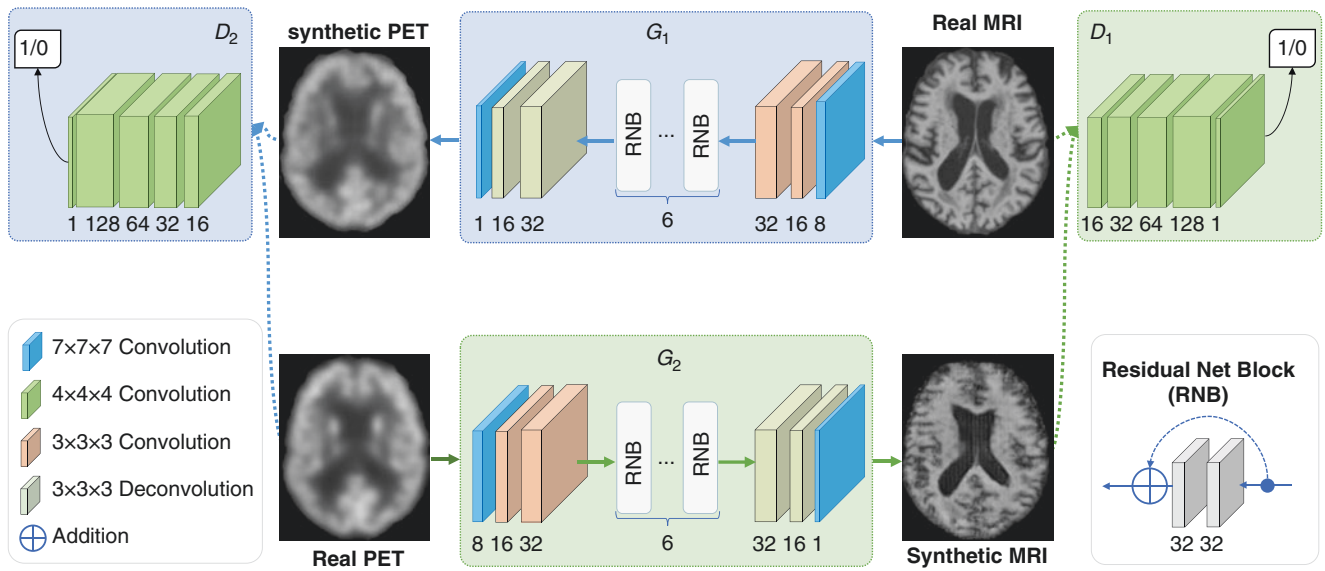


Fig. 9.2 Illustration of the hybrid generative adversarial network (HGAN) for MRI-based PET image synthesis, including two image generators (i.e., G_1 and G_2) and two adversarial discriminators (i.e., D_1 and D_2)

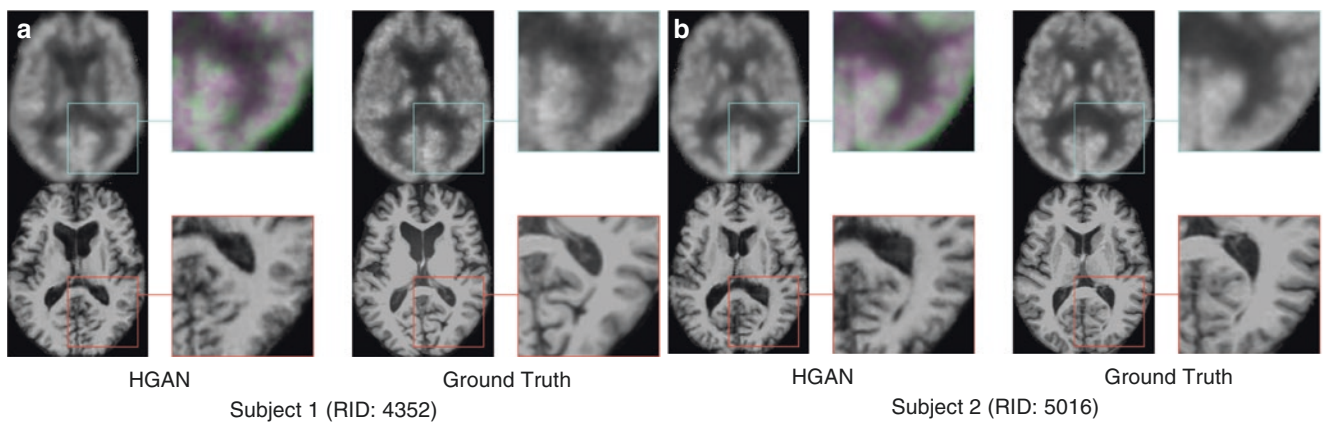


Fig. 9.3 Illustration of synthetic (Syn.) PET/MRI generated by HGAN for two typical subjects (Roster IDs: 4352, 5016), as well as their corresponding real PET/MRI images

conveyed in multi-modality neuroimaging data. Here, the disease-image specificity refers to two types of knowledge: (1) not all regions in an MRI/PET scan are associated with a specific brain disease [38], and (2) disease-associated brain regions may differ in different modalities (e.g., MRI and PET) [27, 39]. Existing deep learning methods usually treat all brain regions equally in the image synthesis process ignoring that several regions (e.g., hippocampus and amygdala) are highly associated with AD/MCI [38, 40–42]. Previous studies have shown that disease diagnosis models can implicitly or explicitly capture the disease-image specificity through regions of interest (ROIs) and anatomical landmarks [30, 35, 41]. To model the disease-image specificity, it is desirable to integrate disease diagnosis and image synthesis into a unified

framework by imputing missing neuroimages in a diagnosis-oriented manner.

To this end, Pan et al. [43] proposed a disease-image-specific deep learning framework for joint disease diagnosis and image synthesis using incomplete MRI and PET scans. As shown in Fig. 9.4a, this method contained two single-modality Disease-image-Specific Network (DSNet) for MRI-based and PET-based disease diagnosis and a feature-consistent generative adversarial network (FGAN) for image synthesis. A disease-image specific network (DSNet) encoded disease-image specificity in MRI-based and PET-based feature maps (via \mathbb{F}_A and \mathbb{F}_B) to assist the training of FGAN, while FGAN imputed missing images to improve the diagnostic performance of DSNet. Since DSNet and FGAN were trained jointly, missing neuroimages were synthesized in a diagnosis-oriented

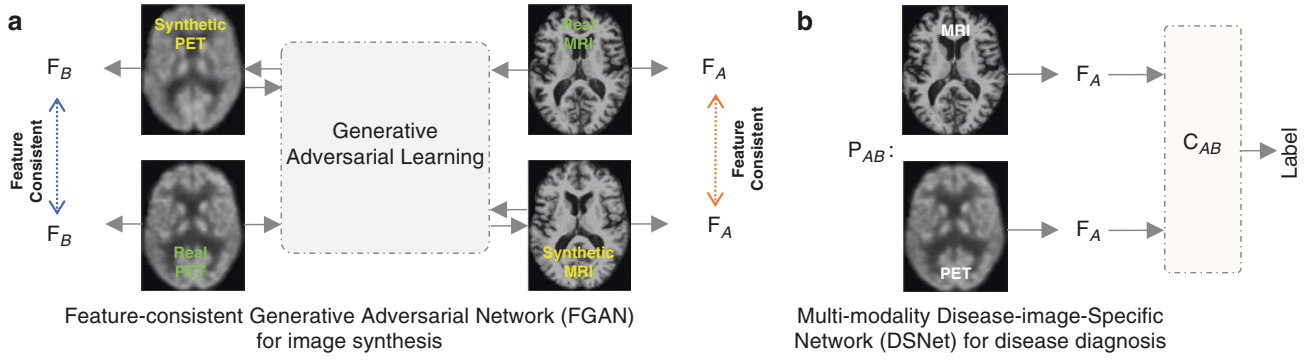


Fig. 9.4 Illustration of a disease-image-specific deep learning framework. (a) A feature-consistent generative adversarial network (FGAN) for image synthesis, encouraging feature maps (e.g., generated by \mathbb{F}_A) of a synthetic image and its real image to be consistent. Based on com-

plete (after imputation) paired MRI and PET scans, a multi-modality DSNet (i.e., $\mathbb{P}_{AB} = [\mathbb{F}_A, \mathbb{F}_B] + \mathbb{C}_{AB}$) is designed for brain disease identification (b). The feature extractors (e.g., \mathbb{F}_A and \mathbb{F}_B) in (b) are followed by a spatial cosine module (e.g., \mathbb{C}_{AB}) for classification

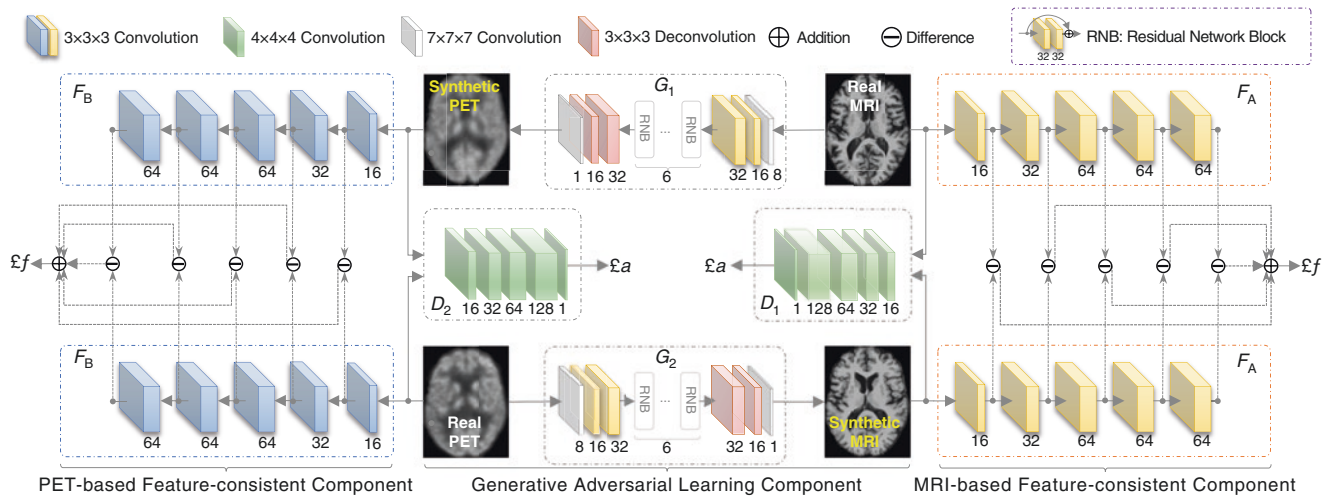


Fig. 9.5 Illustration of a feature-consistent generative adversarial network (FGAN) for image synthesis, including (1) a feature-consistent component (i.e., MRI-based \mathbb{F}_A and PET-based \mathbb{F}_B) and (2) a genera-

tive adversarial learning component, with two image generators (i.e., G_1 and G_2) and two adversarial discriminators (i.e., D_1 and D_2)

manner. Using complete MRI and PET scans (after imputation), automated disease diagnosis was performed via DSNet, as shown in Fig. 9.4b. More details on the architecture of DSNet can be found elsewhere [43].

The network architecture of FGAN is illustrated in Fig. 9.5. The FGAN model contained two feature-consistent components (i.e., MRI-based \mathbb{F}_A and PET-based \mathbb{F}_B) to encourage (1) feature maps of a synthetic image to be consistent with those of its corresponding real image and (2) a generative adversarial learning component to synthesize images under the constraints of feature consistency (i.e., \mathcal{L}_f) and distribution consistency (i.e., \mathcal{L}_a). Note that \mathbb{F}_A and \mathbb{F}_B were learned in MRI-based and PET-based DSNet models, respectively, through which the disease-image specificity learned in DSNet was employed in the image synthesis process, encouraging FGAN to focus on those disease-associated regions in each modality. The adversarial discriminators, i.e.,

D_1 and D_2 , were used to constrain the synthetic MRI and PET scans to follow the same data distribution of those real MRI and PET scans, respectively. Besides, two generators (i.e., G_1 and G_2) were learned to construct bi-directional mappings between two imaging modalities. By jointly training DSNet and FGAN, one encourages that disease-image specificity learned by DSNet can be preserved in the image synthesis process and synthetic images are task-oriented for disease diagnosis.

Based on ADNI-1 and ADNI-2, two generative models were compared with FGAN, including (1) a conventional GAN with only the adversarial loss and (2) the cycle-consistent GAN (CGAN) [32]. These three models (i.e., GAN, CGAN, and FGAN) were trained on subjects with MRI and PET scans in ADNI-1 and tested on subjects with both MRI and PET scans in ADNI-2. Three metrics were used to measure the quality of synthetic images gen-

Table 9.1 Results of image synthesis achieved by different methods for MRI and PET in ADNI-2, with the models trained on ADNI-1

Method	Synthetic MRI					Synthetic PET				
	MAE (%)	SSIM (%)	PSNR	AUC ¹ (%)	AUC ² (%)	MAE (%)	SSIM (%)	PSNR	AUC ¹ (%)	AUC ² (%)
GAN	15.03	55.56	23.48	66.83	53.64	11.62	55.27	27.13	52.92	51.54
CGAN	14.09	59.38	23.96	71.00	57.20	10.70	58.15	27.16	57.50	52.55
FGAN	12.61	64.04	25.10	92.98	77.61	8.03	68.17	29.62	83.80	71.27

erated by different methods, including (1) the mean absolute error (MAE), (2) peak signal-to-noise ratio (PSNR) [44], and (3) structural similarity index measure (SSIM). The experimental results are shown in Table 9.1. To further evaluate the reliability of synthetic MR and PET images (generated by FGAN) in disease diagnosis, values of the area under the receiver operating characteristic (AUC) achieved by DSNet in two diagnosis tasks, i.e., AD vs. HC classification (with results denoted as AUC¹) and MCI conversion prediction (with results denoted as AUC²), are also found in Table 9.1. This table suggests that FGAN can generate high-quality MRI and PET scans in terms of three metrics and that the AUC values obtained by using FGAN-based synthetic images are significantly better than those using CGAN-based and GAN-based synthetic images. This implies that FGAN is effective in generating diagnosis-oriented images.

Future Research Direction

Several technical issues need to be considered in the future. First, even though existing methods [43] can automatically locate disease-related regions to help image synthesis, those regions are only coarsely defined. It is interesting to identify finer regions in the brain image for further improvement. Also, multi-modal neuroimaging data used in existing studies were usually acquired from different imaging sites, and data from different sites may follow different distributions. It is desirable to alleviate the negative influences of different data distributions via data harmonization approaches, e.g., data adaptation techniques [45, 46].

Conclusion

PET/MR has already demonstrated great potentials in both clinical and research applications. The recent advances of instrumental, software, and AI developments contribute to a significant improvement of PET performance, which leads to improved image SNR, reduced scan time, and lower radio-tracer dose. We believe that the technology of PET/MR technology will be continuously progressing, and its role in clinical practice will keep growing.

References

1. Surti S, Karp JS. Current status of PET technology. In: Zhang J, Knopp MV, editors. *Advances in PET: the latest in instrumentation, technology, and clinical practice*. Cham: Springer International Publishing; 2020. p. 3–14.
2. Cherry SR, Badawi RD, Karp JS, Moses WW, Price P, Jones T. Total-body imaging: transforming the role of positron emission tomography. *Sci Transl Med*. 2017;9(381):eaaf6169.
3. Tan H, Gu Y, Yu H, Hu P, Zhang Y, Mao W, et al. Total-body PET/CT: current applications and future perspectives. *AJR Am J Roentgenol*. 2020;215(2):325–37.
4. Cherry SR, Jones T, Karp JS, Qi J, Moses WW, Badawi RD. Total-body PET: maximizing sensitivity to create new opportunities for clinical research and patient care. *J Nucl Med*. 2018;59(1):3–12.
5. Ordonez AA, Sellmyer MA, Gowrishankar G, Ruiz-Bedoya CA, Tucker EW, Palestro CJ, et al. Molecular imaging of bacterial infections: overcoming the barriers to clinical translation. *Sci Transl Med*. 2019;11(508):eaax8251.
6. Dubroff JG, Doot RK, Falcone M, Schnoll RA, Ray R, Tyndale RF, et al. Decreased nicotinic receptor availability in smokers with slow rates of nicotine metabolism. *J Nucl Med*. 2015;56(11):1724–9.
7. Cavaliere C, Tramontano L, Fiorenza D, Alfano V, Aiello M, Salvatore M. Gliosis and neurodegenerative diseases: the role of PET and MR imaging. *Front Cell Neurosci*. 2020;14:75.
8. Vandenberghe S, Mikhaylova E, D’Hoe E, Mollet P, Karp JS. Recent developments in time-of-flight PET. *EJNMMI Phys*. 2016;3(1):3.
9. Yamaguchi S, Wagatsuma K, Miwa K, Ishii K, Inoue K, Fukushima M. Bayesian penalized-likelihood reconstruction algorithm suppresses edge artifacts in PET reconstruction based on point-spread-function. *Phys Med*. 2018;47:73–9.
10. Beyer T, Lassen ML, Boellaard R, Delso G, Yaqub M, Sattler B, et al. Investigating the state-of-the-art in whole-body MR-based attenuation correction: an intra-individual, inter-system, inventory study on three clinical PET/MR systems. *MAGMA*. 2016;29(1):75–87.
11. Chen Y, An H. Attenuation correction of PET/MR imaging. *Magn Reson Imaging Clin N Am*. 2017;25(2):245–55.
12. Sekine T, Buck A, Delso G, Ter Voert EE, Huellner M, Veit-Haibach P, et al. Evaluation of atlas-based attenuation correction for integrated PET/MR in human brain: application of a head atlas and comparison to true CT-based attenuation correction. *J Nucl Med*. 2016;57(2):215–20.
13. Sekine T, Ter Voert EE, Warnock G, Buck A, Huellner M, Veit-Haibach P, et al. Clinical evaluation of zero-Echo-time attenuation correction for brain 18F-FDG PET/MRI: comparison with atlas attenuation correction. *J Nucl Med*. 2016;57(12):1927–32.
14. Wiesinger F, Bylund M, Yang J, Kaushik S, Shanbhag D, Ahn S, et al. Zero TE-based pseudo-CT image conversion in the head and its application in PET/MR attenuation correction and MR-guided radiation therapy planning. *Magn Reson Med*. 2018;80(4):1440–51.
15. Mackewn JE, Stirling J, Jeljeli S, Gould SM, Johnstone RI, Merida I, et al. Practical issues and limitations of brain attenuation correction on a simultaneous PET-MR scanner. *EJNMMI Phys*. 2020;7(1):24.

16. Inomata T, Watanuki S, Odagiri H, Nambu T, Karakatsanis NA, Ito H, et al. A systematic performance evaluation of head motion correction techniques for 3 commercial PET scanners using a reproducible experimental acquisition protocol. *Ann Nucl Med*. 2019;33(7):459–70.
17. Catana C, Benner T, van der Kouwe A, Byars L, Hamm M, Chonde DB, et al. MRI-assisted PET motion correction for neurological studies in an integrated MR-PET scanner. *J Nucl Med*. 2011;52(1):154–61.
18. Gillman A, Smith J, Thomas P, Rose S, Dowson N. PET motion correction in context of integrated PET/MR: current techniques, limitations, and future projections. *Med Phys*. 2017;44(12):e430–e45.
19. Slipsager JM, Ellegaard AH, Glimberg SL, Paulsen RR, Tisdall MD, Wighton P, et al. Markerless motion tracking and correction for PET, MRI, and simultaneous PET/MRI. *PLoS One*. 2019;14(4):e0215524.
20. Kyme AZ, Aksoy M, Henry DL, Bammer R, Maclaren J. Marker-free optical stereo motion tracking for in-bore MRI and PET-MRI application. *Med Phys*. 2020;47(8):3321–31.
21. Zaharchuk G. Next generation research applications for hybrid PET/MR and PET/CT imaging using deep learning. *Eur J Nucl Med Mol Imaging*. 2019;46(13):2700–7.
22. Gong K, Yang J, Kim K, El Fakhri G, Seo Y, Li Q. Attenuation correction for brain PET imaging using deep neural network based on Dixon and ZTE MR images. *Phys Med Biol*. 2018;63(12):125011.
23. Wang Y, Yu B, Wang L, Zu C, Lalush DS, Lin W, et al. 3D conditional generative adversarial networks for high-quality PET image estimation at low dose. *Neuroimage*. 2018;174:550–62.
24. Xiang L, Qiao Y, Nie D, An L, Wang Q, Shen D. Deep auto-context convolutional neural networks for standard-dose PET image estimation from low-dose PET/MRI. *Neurocomputing*. 2017;267:406–16.
25. Wang Y, Shen D, Ma G, An L, Shi F, Zhang P, et al. Semisupervised triple dictionary learning for standard-dose PET image prediction using low-dose PET and multimodal MRI. *IEEE Trans Biomed Eng*. 2017;64(3):569–79.
26. Xu J, Gong E, Ouyang J, Pauly J, Zaharchuk G. Ultra-low-dose 18F-FDG brain PET/MR denoising using deep learning and multi-contrast information: SPIE; 2020.
27. Liu M, Zhang J, Yap PT, Shen D. View-aligned hypergraph learning for Alzheimer's disease diagnosis with incomplete multi-modality data. *Med Image Anal*. 2017;36:123–34.
28. Parker R. Missing data problems in machine learning: VDM Verlag; 2010.
29. Jack CR Jr, Bernstein MA, Fox NC, Thompson P, Alexander G, Harvey D, et al. The Alzheimer's Disease Neuroimaging Initiative (ADNI): MRI methods. *J Magn Reson Imaging*. 2008;27(4):685–91.
30. Liu M, Zhang J, Adeli E, Shen D. Landmark-based deep multi-instance learning for brain disease diagnosis. *Med Image Anal*. 2018;43:157–68.
31. Sterne JA, White IR, Carlin JB, Spratt M, Royston P, Kenward MG, et al. Multiple imputation for missing data in epidemiological and clinical research: potential and pitfalls. *BMJ*. 2009;338:b2393.
32. Zhu J-Y, Park T, Isola P, Efros AA, editors. Unpaired image-to-image translation using cycle-consistent adversarial networks. *IEEE*; 2017.
33. Beckmann M, Lloyd AJ, Haldar S, Fave G, Seal CJ, Brandt K, et al. Dietary exposure biomarker-lead discovery based on metabolomics analysis of urine samples. *Proc Nutr Soc*. 2013;72(3):352–61.
34. Krizhevsky A, Sutskever I, Hinton GE, editors. ImageNet classification with deep convolutional neural networks. *NIPS*; 2012.
35. Liu M, Zhang J, Nie D, Yap PT, Shen D. Anatomical landmark based deep feature representation for MR images in brain disease diagnosis. *IEEE J Biomed Health Inform*. 2018;22(5):1476–85.
36. Pan Y, Liu M, Lian C, Xia Y, Shen D. Spatially-constrained fisher representation for brain disease identification with incomplete multi-modal neuroimages. *IEEE Trans Med Imaging*; 2020.
37. Pan Y, Liu M, Lian C, Zhou T, Xia Y, Shen D, editors. Synthesizing missing PET from MRI with cycle-consistent generative adversarial networks for Alzheimer's disease diagnosis. Cham: Springer International Publishing; 2018.
38. Lian C, Liu M, Zhang J, Shen D. Hierarchical fully convolutional network for joint atrophy localization and Alzheimer's disease diagnosis using structural MRI. *IEEE Trans Pattern Anal Mach Intell*. 2020;42(4):880–93.
39. Cheng B, Liu M, Zhang D, Munsell BC, Shen D. Domain transfer learning for MCI conversion prediction. *IEEE Trans Biomed Eng*. 2015;62(7):1805–17.
40. Wachinger C, Salat DH, Weiner M, Reuter M. Alzheimer's disease neuroimaging I. Whole-brain analysis reveals increased neuroanatomical asymmetries in dementia for hippocampus and amygdala. *Brain*. 2016;139(Pt 12):3253–66.
41. Zhang D, Shen D. Alzheimer's disease neuroimaging I. Multi-modal multi-task learning for joint prediction of multiple regression and classification variables in Alzheimer's disease. *Neuroimage*. 2012;59(2):895–907.
42. Cuingnet R, Gerardin E, Tessieras J, Auzias G, Lehericy S, Habert MO, et al. Automatic classification of patients with Alzheimer's disease from structural MRI: a comparison of ten methods using the ADNI database. *Neuroimage*. 2011;56(2):766–81.
43. Pan Y, Liu M, Lian C, Xia Y, Shen D, editors. Disease-image specific generative adversarial network for brain disease diagnosis with incomplete multi-modal neuroimages. Cham: Springer International Publishing; 2019.
44. Hore A, Ziou D, editors. Image quality metrics: PSNR vs. SSIM. *IEEE*; 2010.
45. Zhang J, Liu M, Pan Y, Shen D. Unsupervised conditional consensus adversarial network for brain disease identification with structural MRI. Cham: Springer International Publishing; 2019.
46. Wang M, Zhang D, Huang J, Yap PT, Shen D, Liu M. Identifying autism spectrum disorder with multi-site fMRI via low-rank domain adaptation. *IEEE Trans Med Imaging*. 2020;39(3):644–55.

Index

- A**
- A β imaging
 - in AD, 103–105
 - in dementias, 105
 - PET/MRI, 106
 - A β plaques, 99
 - Absent comma sign, 295
 - Acetylcholine esterase inhibitor (AChEI), 452
 - Acetylcholinesterase (AChE) inhibitors, 180, 182, 183
 - Acinic cell carcinoma, 690
 - Activities of daily living (ADLs), 452, 453
 - Acute ischemic stroke (AIS)
 - intracerebral hemorrhage, 209–211
 - metabolic changes, 207, 208
 - tissue function and viability, 208, 209
 - Acute suppurative sialadenitis, 697
 - Adenoid cystic carcinoma (ACC), 690
 - Agrammatic variant of PPA (PPA-G), 253
 - Alien hand syndrome, 239
 - Alpha-synuclein, 291, 361
 - α -synucleinopathies, 291
 - ALS revised functional rating scale (ALS-FRS-R), 397
 - Altered glucose metabolism, 89
 - Altered intracellular metabolism, 89, 90
 - Alzheimer's disease (AD), 248
 - abnormal changes, 68
 - advanced medial temporal lobe atrophy, 258
 - AT(N) Biomarker Grouping, 268
 - Braak staging, 258
 - brain metabolic features, 69, 70
 - cholinesterase system, 180
 - clinical cases, 248
 - clinical presentation, 257, 258
 - cognitive and behavioral symptoms, 248
 - deep belief network, 68
 - deep learning model, 68, 69
 - diagnostic criteria, 268
 - disease genetics, 268
 - epidemiology, 257
 - ^{18}F labeled radiopharmaceuticals targeting brain amyloid deposits, 68
 - glymphatic system
 - animal studies, 850
 - contrast agent concentration, 851, 854
 - diffusion-weighted imaging, 858
 - intrathecal contrast-enhanced MRI, 856, 858
 - pharmacokinetic models, 854–857
 - qualitative MRI studies, 851, 852
 - role of, 849, 850
 - hallmark neuropathologic changes, 68
 - imaging features
 - advanced medial temporal lobe atrophy, 258
 - functional imaging, 259
 - molecular imaging, 259, 260, 263–267
 - structural imaging, 258
 - imaging hallmarks, 258
 - microglial activation, 193
 - mortality, 257
 - neuropathological hallmarks, 268
 - neuropathology, 849
 - prevalence, 248
 - prevalence, 67
 - Tau imaging, 115–117
 - treatment, 269
 - Alzheimer's Disease Neuroimaging Initiative (ADNI) database, 70
 - Alzheimer's disease (AD), 416
 - application of, 99
 - A β imaging, 103–105
 - A β plaques, 99
 - characterization, 99
 - ^{11}C -PiB and ^{18}F -labeled tracers, 100, 101
 - definition, 99
 - diagnosis, 99
 - misfolded protein aggregation, 99
 - pathogenesis, 99
 - pathological hallmarks, 99
 - pathophysiological stages, 99
 - preclinical, 105
 - Alzheimer's Disease Neuroimaging Initiative (ADNI-1), 81
 - American Joint Committee on Cancer (AJCC)/Union for International Cancer Control (UICC) cancer staging, 627, 628
 - Amino acid (AA) PET/MRI
 - chemical structure, 137, 138
 - clinical significance, 140–142
 - [^{11}C]-MET, 141
 - AA transporter system L vs. system A, 146, 148
 - biopsy guidance, 146
 - brain tumor differentiation, grading, and prognosis, 141–143
 - neuronavigation, 146
 - oligodendrogliomas, 144
 - treatment response assessment, 146
 - tumor delineation, 145
 - tumor recurrence versus treatment-related changes, 144, 145
 - [^{18}F]-DOPA
 - clinical applications, 157
 - evaluation, 154
 - limitation, 154
 - non-invasive genetic profiling, 157
 - oncologic and non-oncologic diseases, 154
 - recurrence vs. treatment-related changes, 155, 156
 - true tumor delineation and metabolic activity assessment, 155
 - tumor detection and grading, 155

- Amino acid (AA) PET/MRI (*cont.*)
 - tumor genotyping, 157
- [¹⁸F]-FET, 146
 - biochemical characteristics, 146
 - dynamic, 147, 150, 151
 - early response to treatment, 151, 152
 - machine learning, 154
 - non-invasive genetic profiling, 153
 - photopenic defect, 153, 154
 - static, 147
 - tumor genotyping, 153
 - tumor grading, 151
 - tumor progression vs. treatment-related changes, 152, 153
 - unique feature of, 146
- [¹⁸F]-Fluciclovine
 - border delineation, 158
 - clinical application, 160
 - neuronavigation, 158
 - predicting tumor grade, 158, 159
 - tumor detection, 158
 - tumor recurrence vs. treatment-related changes, 159–161
- metabolism and cancer, 140
- technical imaging aspects, 148–150
- tracers, 143
- transporters, 137
 - across BBB and tumor uptake, 137
 - and uptake, 139, 140
 - ASCT, subtypes, 138
 - LAT, subtypes, 138
 - Na⁺-dependent transporters, 137
 - principles, 139, 140
 - System L transporters, 137
- Amnesic episodes, 228
- Amnesic mild cognitive impairment (aMCI), 473
- Amyloid imaging
 - clinical applications, 101–103
 - tracer, 99, 100
 - visual assessment, 101
- Amyloid PET tracer, 100
- Amyloid precursor protein (APP), 481
- Amyloid/tau imaging, 52–55
- Amyloid-related imaging abnormalities (ARIA) edema, 280
- Amyotrophic lateral sclerosis (ALS)
 - ¹¹C-flumazenil PET, 405
 - diagnosis, 397, 398
 - diffusion tensor imaging, 404
 - ¹⁸F-FDG PET, 405, 406
 - limb-onset signs and symptoms, 397
 - magnetic resonance imaging, 398
 - bulbar-onset ALS, 398, 401
 - linear T2 hyperintensity, 398, 403
 - progression of iron deposition, 398, 402
 - structural mimics, 398
 - SWI and QSM, 398–400
 - magnetic resonance imaging spectroscopy, 404
 - pathophysiology, 397
 - TSPO, 406
 - voxel-based morphometry, 398, 404
- Amyotrophic lateral sclerosis-frontotemporal spectrum disorder (ALS-FTSD), 397
- Anaplastic ependymoma, 551
- Anaplastic oligodendroglioma, 540
- Aneurysm, 793–797
- Angiocentric lymphoma, 560
- Antidepressants-tricyclic antidepressants (TCAs), 232
- Arterial input function (AIF), 828, 829
- Arterial spin labeling (ASL), 198, 495, 528, 839, 840
 - modifiable daily lifestyle behaviors, 60
 - obesity, 58
- Arterial spin labeling (ASL-MR), 307, 309
- Arteriovenous malformations (AVMs), 798, 799
- Artificial intelligence (AI)
 - ADNI database, 82
 - advanced techniques, 81
 - in Alzheimer's disease, 67
 - ¹⁸F labeled radiopharmaceuticals targeting brain amyloid deposits, 68
 - abnormal changes, 68
 - brain metabolic features, 69, 70
 - deep belief network, 68
 - deep learning model, 68, 69
 - hallmark neuropathologic changes, 68
 - prevalence, 67
 - cerebrovascular disease, 76, 77
 - characteristics, 67
 - computer-aided disease diagnosis model, 81, 82
 - deep learning methods, 81
 - deep machine learning, 40
 - definition, 67
 - disease image specific GAN, 82, 83
 - disease-image-specific deep learning framework, 83, 84
 - disease-related anatomical landmarks, 81
 - ([¹⁸F]-FET), 154
 - hybrid GAN, 82, 83
 - image synthesis, 85
 - multi-modal neuroimaging data, 85
 - neuro-oncology, 74, 75
 - in Parkinson disease
 - atypical parkinsonian syndromes, 73, 74
 - early diagnosis, 70–72
 - early differentiation of, 73, 74
 - PET/MR, 81
 - problem formulation, 81
- Artificial neural networks (ANNs), 67
- Astrocytic tumors
 - desmoplastic infantile tumors, 548
 - dysembryoplastic neuroepithelial tumor, 547
 - dysplastic cerebellar gangliocytoma, 548
 - embryonal tumors, 548, 550
 - gangliocytoma, 547
 - gangliogliomas, 547
 - neuronal and mixed neuronal-glioma tumors, 546
 - pilocytic astrocytomas, 545
 - pleomorphic xanthoastrocytomas, 546
- Astrocytoma, 714, 765–767
- Astrocytoma, IDH-mutant, 541, 542
- Atlas-based approaches, 20, 21
- Atlas-based methods, 80
- Attenuation correction (AC)
 - attenuated and non-attenuated photon intensity, 17
 - attenuation correction maps, 17
 - direct-image based approaches, 19–21
 - MR-based attenuation correction, 21
 - non-AC vs. AC PET image, 17
 - in PET/MR, 18, 19
 - photon transmission, 17
 - quantitative errors, 17
 - specific extrapolation techniques-low energy attenuation maps, 17
 - using transmission image, 17
- Attenuation correction maps, 17
- Atypical choroids plexus papilloma, 552
- Atypical infections, 602
- Atypical parkinsonian syndromes (APS), 73, 74, 352, 373, 430, 431
- Atypical teratoid/rhabdoid tumors (ATRT), 550

- Autocorrelation and Fisher scoring algorithms, 72
 Autoimmune encephalitis, 231
 Autoimmune epilepsy (AE), 511, 513–515
 Autosomal dominant Alzheimer's disease (ADAD), 104
 Avalanche photodiode (APD), 5
 Axial diffusivity (AD), 787
 Axial spondylarthritis (axSpA), 728, 729
 Axial spondyloarthritis, 728, 729
- B**
 Bayesian Penalized Likelihood Image Reconstruction, 80
 Behavioral rigidity, 304
 Behavioral variant of a frontotemporal dementia (bvFTD), 105, 252
 vs. AD, 304
 ASL-MR, 309
 clinical scales and diagnostic criteria, 304
 dehavioral rigidity, 304
 disease course, 304
 DTI, 309
 epidemiology, 303
 fMRI, 309
 genetics, 303, 304
 histopathologic diagnostic criteria, 304, 305
 hybrid PET/MR, 309
 MRI, 305, 306
 pathologic diagnosis, 304
 PET, 306–309
 phenocopy syndrome, 304
 physical examination, 304
 subtypes, 304
 symptoms and disease course, 304
 treatment and therapeutics research, 310
 Benson's syndrome, see Posterior cortical atrophy (PCA)
 β -amyloid assessment methodologies, 101
 β -amyloid positive PET image assessment, 101
 β -secretase (BACE), 481
 BFCN ACh system, 179
 Big Data, 67
 Binding potential (BP), 24
 Black boxes, 68
 Blood pressure (BP) management, 453
 Blood–brain barrier (BBB), 168, 448, 449, 839
 Blood-oxygen-level-dependent (BOLD) signal, 451
 Braak staging system, 292, 293
 Brain abscess, 607–609
 Brain COMPASS™, 80
 Breast cancer, 660
- C**
 CAA-related inflammation syndrome (CAA-ri), 280
 Callosal angle (CA), 461
 Cancer with unknown primary (CUP), 640
 Capillary telangiectasias, 802
 Carotid Occlusion Surgery Study (COSS), 207
¹¹C-BF-227 (BF227), 100
 [¹¹C]-dihydrotrabenazine (DTBZ) PET, 366, 423
 Central executive network (CEN), 452
 Central nervous system (CNS) tumors
 esthesioneuroblastoma, 220, 221
 hemangioblastoma, 221
 medulloblastoma, 221
 meningiomas, 217, 218
 in metastatic disease, 223
 paragangliomas, 218, 220
 pituitary adenomas, 221, 222
 Central neurocytoma, 552
 Cerebral amyloid angiopathy (CAA), 279
 brain MRI findings, 273–275
 definition, 273
 epidemiology, 273
 neuroimaging findings, 278, 279
 pathophysiology, 273
 PET, 274
 A β PET tracers and diagnostic utility, 276, 277
 amyloid PET, CAA MRI markers and vascular imaging modalities, 277, 278
 CAA-specific amyloid-PET imaging, 275, 276
 probable/possible, 273
 sporadic versus hereditary CAA, 273
 Cerebral aneurysms, 795–797
 Cerebral Autosomal dominant arteriopathy with subcortical infarcts and leukoencephalopathy (CADASIL), 808–810
 Cerebral blood flow (CBF)
 acetazolamide, 833, 834
 adenosine, 833, 834
 AIF, 828, 829
 blood-brain partition coefficient, 829
 CBV, 830, 832
 cerebrovascular reactivity, 832
 cerebrovascular reserve capacity, 832
 dipyridamole, 833, 834
 hypercapnia, 833, 834
 kinetic parameters, 828
 permeability surface area product, 829–831
 PET/MRI, 834, 835
 positron-emitting radioactive probes, 827, 828
 Cerebral blood volume (CBV), 830, 832
 Cerebral cavernous venous malformation, 801, 802
 Cerebral hemodynamics, 201, 203–205, 207
 Cerebral microbleeds (CMB), 789, 790
 Cerebral microhemorrhages, 242
 Cerebral venous angioma, 801
 Cerebrovascular basement membrane (CBM), 277
 Cerebrovascular disease, 76, 77, 228
 cerebral hemodynamics, 201, 203–205, 207
 intracerebral hemorrhage, 209–211
 metabolic changes, 207, 208
 tissue function and viability, 208, 209
 Charles-Bonnet syndrome, 229
 Cholinergic system, 367, 368
 Chordoid and glial elements, 554
 Chorea, 238, 417
 Choroid plexus carcinomas, 552
 Choroid plexus papilloma (CPP), 552
 Chronic traumatic encephalopathy (CTE), 481
 Cingulate island sign, 297
 c-Jun N-terminal kinase (JNK), 481
¹¹C-labeled Pittsburg compound B (PiB), 100
 [¹¹C]LSN3172176, 184
¹¹C-methionine (MET), 137, 141, 575
 AA transporter system L vs. system A, 146, 148
 biopsy guidance, 146
 brain tumor differentiation, grading, and prognosis, 141–143
 neuronavigation, 146
 oligodendrogliomas, 144
 transport, 137
 treatment response assessment, 146
 tumor delineation, 145
 tumor recurrence versus treatment-related changes, 144, 145
¹¹C-methionine (MET) PET, 599–601
 CNS cholinergic system

- acetylcholinesterase, 182, 183
 - functional role
 - in attention, 179
 - in memory, 179
 - in reward and motivation, 180
 - in striatum, 180
 - muscarinic receptors
 - [11C]LSN3172176, 184
 - [18F]-FP-TZTP, 184
 - in neuropsychiatric and neurodegenerative disorders
 - in AD, MCI and cognitive decline, 180
 - in striatal function and Schizophrenia, 180
 - in substance abuse and dependence, 180, 181
 - nicotinic receptors
 - $\alpha 4\beta 2^*$, 183
 - $\alpha 7$, 183, 184
 - PET radiotracers, 182
 - quantitative methods, 181
 - radiotracers, 182, 184
 - vesicular acetylcholine transporter, 184, 185
 - CNS histoplasmosis, 602, 604, 605
 - CNS lymphoma, 559
 - Cognitive behavioral therapy (CBT), 288
 - Cognitive decline, 180
 - Cognitive disorders, 67
 - Cognitive impairment, 180, 460
 - Complete response (CR), 589
 - Computer-aided diagnosis system, 81
 - Congenital cranio-cervical malformation, 723, 724
 - Congenital hyperinsulinism (CHI), 774
 - Congenital spinal pathology, 723, 724
 - Connectivity
 - modifiable daily lifestyle behaviors, 61
 - obesity, 59
 - Convexity apparently hyperperfusion (CAPPAAH) sign, 464
 - C9orf72 mutations, 306
 - Corticobasal degeneration (CBD), 228, 250, 421
 - classification, 373
 - clinical criteria, 373
 - clinicopathological syndrome, 373
 - diagnostic criteria, 373
 - functional imaging techniques, 375
 - dopaminergic imaging, 375, 376
 - metabolic imaging, 376–379
 - perfusion imaging, 378, 380
 - tau imaging, 380
 - TSPO imaging studies, 380
 - microscopic characteristics, 373
 - pathology, 373
 - prevalence, 373
 - structural imaging, 373–375
 - Corticobasal ganglionic degeneration, 250
 - Corticobasal syndrome (CBS), 373
 - Count-based H2150/O150 ratio method, 205
 - ^{11}C -PBB3, 354
 - [^{11}C]raclopride, 48
 - Craniopharyngiomas, 554
 - Creutzfeldt-Jakob disease (CJD), 118
 - clinical presentation, 388
 - definitive diagnosis, 387
 - diagnosis, 388, 389
 - epidemiology, 388
 - genetic forms, 387
 - genetics, 388
 - imaging, 389–393
 - treatment, 393
 - Crossed cerebellar diaschisis (CCD)
 - anatomy, 470–472
 - clinical presentation, 472
 - FDG-PET and FLAIR axial views, 474–476
 - hybrid PET/MR brain image acquisition, 474
 - hybrid PET/MR image interpretation, 474
 - neurodegenerative disease, 469, 470
 - prevalence and association, 472, 473
 - [^{11}C]-(R)-PK11195, 380
 - Cryptococcal choroid plexitis, 604, 606
 - Custom-molded headcase, 27
 - Cutaneous melanoma, 657, 658
 - Cycle-consistent generative adversarial network (CGAN), 82
- D**
- Deconvolution-based approach, 30
 - Deep belief network (DBN), 68
 - Deep convolutional neural network, 70
 - Deep convolutional neural network framework (PD Net), 71
 - Deep learning (DL) methods, 67, 81
 - Deep learning model, 68, 69
 - Deep tendon reflexes (DTRs), 237
 - Default-mode network (DMN), 201, 451, 484
 - Degenerative disease
 - IVDD, 724
 - posterior elements, 725
 - vertebral bodies and endplates, 724, 725
 - Degenerative spinal stenosis, 725
 - Delphian node, 658, 659
 - Dementia, 460
 - Dementia with Lewy bodies (DLB), 228, 250, 285
 - causes, 291
 - clinical presentation, 292, 293
 - epidemiology
 - genetics, 292
 - incidence/prevalence, 291, 292
 - pathologic hallmark, 292
 - histopathologic diagnostic criteria
 - non-imaging biomarkers, 293
 - pathology, 293
 - MIBG, 297
 - MRI/CT, 293, 294
 - natural history, 292
 - PET
 - amyloid, 295
 - ^{18}F -DOPA, 294
 - ^{18}F -FDG-PET, 295
 - tau, 295
 - post-synaptic ligands, 297
 - presynaptic ligands, 295, 297
 - treatment, 291, 297, 298
 - Dementias with motor variants, 250
 - clinical cases, 251
 - cognitive and behavioral symptoms, 251
 - corticobasal degeneration, 251
 - progressive supranuclear palsy, 251
 - Depth of invasion (DOI), 630, 632
 - Depth-of-interaction (DOI) measurement, 4
 - Desmoplastic infantile tumors, 548
 - Developmental venous anomaly (DVA), 801
 - Diabetes mellitus (DM), 454
 - Diffuse axonal injury (DAI), 483
 - Diffuse gliomas, 540
 - Diffuse midline glioma, H3K27M-mutant, 543
 - Diffusely infiltrating gliomas

- astrocytoma, IDH-mutant, 541, 542
 - diffuse midline glioma, H3K27M-mutant, 543
 - glioblastoma, 542, 543
 - oligodendrogliomas, 541
 - Diffusion tensor imaging (DTI), 307, 309
 - modifiable daily lifestyle behaviors, 61
 - obesity, 59
 - PCA, 284
 - Digitized data, 67
 - Direct imaging, 21
 - Disease-image-specific deep learning framework, 83, 84
 - Disease-image-specific network (DSNet), 83–85
 - Disproportionately enlarged subarachnoid space hydrocephalus (DESH), 461
 - Distribution volume ratio (DVR), 23
 - “Dixon-VIBE” or “LAVA-FLEX” sequence, 80
 - Dominantly inherited Alzheimer network (DIAN), 104
 - Dominantly inherited Alzheimer’s disease (DIAD), 104
 - Dopamine transporter (DaT), 423
 - Dopaminergic dysfunction, 421
 - Dopaminergic system, 366, 367
 - FDOPA
 - dopamine PET-ligands, 125, 126
 - image interpretation, 126
 - PET/MRI, 130
 - visual assessment, 127
 - Dorsolateral nigral hyperintensity (DNH), 422
 - Down syndrome, 723
 - Dual modality imaging
 - advantages, 35, 36
 - AI deep machine learning, 40
 - challenges, 36
 - components, 36
 - diagnostic accuracy, 35
 - evaluation, 35
 - functional and anatomical scan data, 36
 - functional and molecular-level information, 35
 - functional, anatomical and multiparametric data, 35
 - generalizable sample, 39, 40
 - generated datasets, 36
 - hybrid PET/MR scanner, 35
 - hybrid PET/MR use, 35
 - lower socio-economic status, 36
 - PET/MR vs. PET/CT, 35, 37
 - advantages, 37
 - biophysical and biological effects, 38
 - clinical or research examination, 38
 - contraindication, 39
 - early-onset challenges, 37
 - ferromagnetic materials, 38
 - limitations, 38
 - MR-based attenuation correction maps, 37
 - MRI signal intensities, 37
 - patient diagnostic and therapeutic costs, 39
 - public health and economic considerations, 39
 - risks, 38
 - scan duration, 37
 - structural costs, 39
 - trained staff and higher costs, 39
 - variations of, 38
 - risk of, 36
 - sampling bias, 39, 40
 - Dual ultrashort echo time (DUTE) sequence, 20
 - Dural arteriovenous fistulae (DAVF), 800
 - DUTE histogram-based thresholding models, 20
 - Dynamic acquisition, 22
 - Dynamic contrast enhancement (DCE)
 - method, 841
 - perfusion, 529
 - Dynamic susceptibility contrast (DSC), 840, 841
 - method, 198
 - perfusion, 529
 - Dysembryoplastic neuroepithelial tumor (DNET), 547
 - Dysplastic cerebellar gangliocytoma (DCG), 548
- E**
- Embryonal tumors, 548, 550
 - Encephaloceles, 509–511
 - Encephalotrigeminal angiomas, 500, 501
 - Enzyme replacement therapy (ERT), 805
 - Ependymal tumors, 550, 551
 - Ependymoma, 551, 713–715, 766–768
 - Epilepsy, 92
 - encephaloceles, 509–511
 - FCD, 499, 500, 508, 509
 - fluorodeoxyglucose positron emission tomography, 496
 - hemimegalencephaly, 502–504
 - hippocampal sclerosis, 507, 508
 - hybrid PET/MR examinations, 496, 497
 - limbic encephalitis
 - autoimmune epilepsy, 511, 513–515
 - etiology, 511
 - infectious/viral, 511
 - magnetic resonance imaging, 495
 - neoplasm, 503–505
 - single photon emission computed computerized tomography, 496
 - Sturge-Weber syndrome, 499, 501
 - TLE, 507, 508
 - treatment
 - deep brain stimulation, 522
 - diffusion tensor imaging, 520, 521
 - functional MRI, 520, 522
 - high density electroencephalography, 519
 - intracranial electroencephalography, 519–521
 - magnetic resonance-guided focused ultrasound, 523
 - magnetoencephalography, 519
 - non FDG PET imaging, 523
 - quadrimodal imaging, 523
 - responsive neurostimulation, 522
 - 7 Tesla (7T) MRI, 523
 - vagal nerve stimulation, 522
 - tuberous sclerosis, 500, 502, 503
 - vascular malformations, 509, 510, 512, 513
 - Epstein-Barr virus (EBV), 629
 - Esthesioneuroblastoma (ENB), 220, 221
 - Evans index (EI), 461
 - Ewing sarcoma, 769, 770
 - External lumbar drainage (ELD), 460
 - Extra-axial tumors, 557
- F**
- Fabry disease (FD), 805, 807, 808
 - Faciobrachial dystonic seizures (FBDS), 513
 - ¹⁸F-AV1451 (flortaucipir), 354
 - FDG cortical metabolism, 308
 - Feature-consistent generative adversarial network (FGAN), 83–85
 - [¹⁸F]-FDG PET/MR neuroimaging
 - altered glucose metabolism, 89
 - altered intracellular metabolism, 89, 90
 - [¹⁸F]-FDG PET/MR neuroimaging (*cont.*)

- clinical applications, 91, 92, 97
 - differential diagnosis, 92
 - epilepsy, 92
 - glioma diagnosis, 92
 - neurodegenerative diseases, 91, 92
 - neuro-oncology, 92 (*see* Neuro-oncology)
 - mechanism of, 89, 91
 - ¹⁸F-Florbetaben, 100
 - ¹⁸F-florbetapir, 100
 - F-18 flortaucipir, 369
 - [¹⁸F]-Fluciclovine, 137
 - border delineation, 158
 - clinical application, 160
 - neuronavigation, 158
 - predicting tumor grade, 158, 159
 - tumor detection, 158
 - tumor recurrence vs. treatment-related changes, 159–161
 - 6-[¹⁸F]fluoro-L-dopa (FDOPA) PET, 294, 423
 - ¹⁸F-2-fluoro-2-deoxy-D-glucose (FDG), 450
 - ¹⁸F-fluorodeoxyglucose (18F-FDG) PET, 295, 405, 406
 - F-18 fluoro-deoxy phenylalanine (FDOPA), 48, 137, 366
 - clinical applications, 157
 - evaluation, 154
 - limitation, 154
 - non-invasive genetic profiling, 157
 - oncologic and non-oncologic diseases, 154
 - recurrence vs. treatment-related changes, 155, 156
 - true tumor delineation and metabolic activity assessment, 155
 - tumor detection and grading, 155
 - tumor genotyping, 157
 - ¹⁸F-fluoroethyl-tyrosine (FET), 137, 575
 - ¹⁸F-flutemetamol, 100
 - [¹⁸F]-FP-TZTP, 184
 - ¹⁸F-labeled amyloid tracers, 100
 - ¹⁸F labeled radiopharmaceuticals targeting brain amyloid deposits, 68
 - Fluent or semantic (svPPA) variants, 313
 - (3-fluoropropyl)-2 β -carboxymethoxy-3 β -(4-iodophenyl)nortropane (FP-CIT), 367
 - Focal cortical dysplasia (FCD), 499, 500, 508, 509, 741–743, 745
 - Frontal variant (fvFTD), 252
 - Frontotemporal dementia (FTD), 105
 - phenocopy syndrome, 304
 - spectrum disorders, 313
 - Frontotemporal lobar degeneration (FTLD), 228, 323, 337
 - ¹⁸F-THF5105, 354
 - ¹⁸F-THK5105, 355
 - ¹⁸F-THK523, 354
 - ¹⁸F-THK5317/¹⁸F-THK5117, 354, 355
 - ¹⁸F-THK5351, 354
 - FTLD-Tar DNA binding protein (FTLD-TDP), 320
 - Functional MRI (fMRI), 307, 309
 - Fused in sarcoma (FUS), 305
- G**
- [⁶⁸Ga]-DOTATATE PET
 - CNS tumors
 - esthesioneuroblastoma, 220, 221
 - hemangioblastoma, 221
 - in metastatic disease, 223
 - in pituitary adenomas, 221, 222
 - medulloblastoma, 221
 - meningiomas, 217, 218
 - paragangliomas, 218, 220
 - physiologic avidity, 217
 - role and limitations of, 217
 - SSTR subtypes, 217
 - Gait impairment, 460
 - [⁶⁸Ga]-labeled somatostatin analogs, 217
 - Gamma-aminobutyric acid (GABA), 417, 523
 - Gamma-ray acollinearity, 3
 - Gangliogliomas (GG), 547
 - Gastrointestinal cancer, 660, 661
 - Gated PET motion correction techniques, 29
 - GE's Prospective motion correction (PROMO), 32
 - General electric (GE) method, 21, 80
 - Genetic stroke syndrome
 - CADASIL, 808, 809
 - CARASIL, 809, 810
 - Fabry disease, 805, 807, 808
 - MELAS, 811–813
 - MMD and MMS, 814–816, 818–821
 - RVCL-S, 810, 811
 - Genitourinary cancer, 660, 661
 - Germ cell tumors (GCT), 555
 - Germinomas, 557
 - Giant cell arteritis (GCA), 623
 - Glioblastoma multiforme (GBM), 542, 543
 - Global cerebral atrophy (GCA), 443
 - Glucose hypometabolism, 366, 368
 - Glymphatic imaging studies
 - modifiable daily lifestyle behaviors, 61, 62
 - obesity, 59
 - G-protein-coupled D2 receptor (D2R), 367
 - Granulomatous amebic encephalitis, 604, 606, 607
 - Graphic processing units (GPUs), 67
- H**
- Hardware, 79
 - Head and neck cancers are squamous cell carcinoma (HNSCC)
 - advanced functional techniques, 628, 629
 - AJCC/UICC cancer staging, 627, 628
 - cervical nodal disease assessment, 633, 634
 - CUP, 640
 - disease free survival, 651
 - distant metastasis, 634, 635
 - hypopharynx, 650
 - imaging, 628
 - initial diagnosis, 640
 - larynx, 650, 651
 - limitations, 636
 - nasopharynx, 648, 650
 - non-FDG PET tracers, 635, 636
 - oral cavity, 640, 644
 - oropharynx, 644, 648
 - overall survival, 651
 - positron emission tomography imaging, 651
 - primary tumor assessment
 - Depth of invasion, 630, 632
 - HPV positive and negative tumors, 631, 632
 - initial diagnosis, 629
 - larynx, 632, 634
 - NPC, 629, 631
 - oral cavity, 630
 - oropharyngeal SCC, 630, 631, 633
 - sinonasal region, 629, 630
 - T staging, 629
 - risk factors, 627
 - synchronous second primary malignancy, 635
 - T staging subsites, 640
 - Head and neck paraganglioma (HNPG) detection, 220, 716
 - Hemangioblastoma (HMB), 221, 559, 714
 - Hemangiopericytomas, 558

- Hemimegalencephaly, 502–504
 Hereditary cerebral hemorrhage with amyloidosis-Dutch type (HCHWA-D), 273
 Hippocampal atrophy, 807
 Hippocampal sclerosis (HS), 507, 508
 Homeostasis (defense and repair), 50, 52, 53
 HSV encephalitis, 602, 603
 5-HT1 receptors
 5-HT1A receptor radioligands, 168, 169
 5-HT1B receptor radioligands, 168, 169
 5-HT1D, E, F receptors, 169
 5-HT1A receptor radioligands, 168, 169
 5-HT1B receptor radioligands, 168, 169
 5-HT1D, E, F receptors, 169
 5-HT2 receptor radioligands
 5-HT2B receptors, 170
 5-HT2C receptors, 170
 5-HT3 receptors, 170
 5-HT2B receptors, 170
 5-HT2C receptors, 170
 5-HT3 receptors, 170
 5-HT4 receptor radioligands, 170
 5-HT5 receptor radioligands, 170
 5-HT6 receptor radioligands, 170, 171
 5-HT7 receptor radioligands, 171
 Huntingtin (HTT), 411
 Huntington's disease (HD), 228
 adenosine, 416
 age of onset, 411
 CB1 cannabinoid receptor, 416
 cerebral blood flow, 414, 415
 clinical features, 412
 dopaminergic system, 414, 416
 GABA, 417
 glucose metabolism, 414, 415
 magnetic resonance imaging, 412–414
 metabolic abnormalities, 412
 microglial activation, 416
 opioid receptors, 416
 pathophysiology, 411, 412
 PDE10A, 416
 positron emission tomography, 414
 prevalence, 411
 treatment, 417
 Hybrid GAN (HGAN), 82, 83
 6-Hydroxydopamine (6-OHDA)-induced PD rat model, 432
 Hypercapnia, 833, 834
 Hypercholesterolemia/dyslipidemia, 454
 Hypertension, 453, 454
 Hypometabolism, 285
 Hypothalamic/chiasmatic astrocytoma, 554
- I**
 Iatrogenic CJD (iCJD), 387
 Idiopathic normal pressure hydrocephalus (iNPH), see Normal pressure hydrocephalus (NPH)
 Idiopathic RBD (iRBD), 426, 427
¹²³I-FP-CIT SPECT imaging, 70
 [¹²³I]Ioflupane, 48
 Ill-defined margins, 695, 696
 Image-derived arterial input function (IDAIF), 198
 Image-derived input function (IDIF), 829
 I¹²³MIBG myocardial scintigraphy, 297
 Immunological disease, 231
 Immunotherapy RANO (iRANO), 593
 Indifferent uptake pattern, 153
- Inflammatory orbital pseudotumor (IOP), 679
 Intervertebral disc degeneration (IVDD), 724
 Intervertebral fibrous cartilages, 724
 Intracellular metabolism of glucose, 89
 Intracranial mass
 accurate pathological diagnosis, 532, 533
 amino acids, 530, 531
 computed tomography, 527
 FDG, 530, 531
 hybrid PET/MRI technique, 532
 machine learning techniques, 532
 magnetic resonance imaging
 amide proton transfer, 530
 ASL, 528
 conventional sequences, 527, 528
 DCE perfusion, 529
 deuterium MRSI, 530
 diffusion techniques, 530
 DSC perfusion, 529
 functional MRI, 530
 hyperpolarized (1-¹³C) pyruvate, 530
 IVIM, 528
 MR fingerprinting, 530
 MR spectroscopy, 529, 530
 perfusion techniques, 528
 susceptibility imaging, 528
 neoplastic vs. non-neoplastic pathologies, 532
 post-treatment changes vs. residual/recurrent tumor, 533, 534
 prognosis, 535
 radiogenomics, 532
 radiomics, 532
 SSTR, 531, 532
 tumoral infiltration, 532
 Intracranial tumors
 combined PET-MRI, 580–582
 computed tomography, 579, 580
 conventional MRI techniques, 579, 580
 diffusion tensor imaging, 579, 580
 functional MRI, 580
 MR spectroscopy, 580
 perfusion imaging, 580
 positron emission tomography, 581
 pre-radiation planning, 581, 584
 pre-surgical planning, 581, 583
 Intractable seizures, 499, 500
 Intraventricular masses
 central neurocytoma, 552
 chordoid and glial elements, 554
 choroid plexus tumors, 552
 CNS lymphoma, 559
 craniopharyngiomas, 554
 ependymal tumors, 550, 551
 extra-axial tumors, 557
 germ cell tumors, 555
 germinomas, 557
 hemangioblastomas, 559
 hemangiopericytoma/solitary fibrous tumor, 558
 hypothalamic/chiasmatic astrocytoma, 554
 Langerhans cell histiocytosis, 560
 meningiomas, 554, 558
 nongerminomatous tumors, 557
 pineal parenchymal tumors, 555
 pineal tumors, 554
 pituitary adenomas, 554
 primary melanocytic lesions, 559
 sellar/central skull base region, 554
 Intravoxel incoherent motion (IVIM), 528

Investigational New Drug (IND) application, 13, 14
 Investigators brochure (IB), 13
 Ischemic cerebrovascular disease, 241

K

18 kDa translocator protein (TSPO), 191–194, 368
 KinetiCor, 29
 Klippel Feil syndrome, 723, 724

L

Landmark-based multi-modal multi-instance learning method (LDMIL), 82
 Langerhans cell histiocytosis (LCH), 560, 771, 773
 Language-variant frontotemporal dementias (lvFTD), 252, 313
 Large amino acid transporters (LAT), 137
 L3,4-dihydroxy-6-[18F]fluoro-L-phenylalanine (FDOPA)
 in dopaminergic system
 dopamine PET-ligands, 125, 126
 image interpretation, 126
 PET/MRI, 130
 visual assessment, 127
 in neuro-oncology
 aminoacid tracer, 121, 122
 and PET/MRI, 123
 image interpretation, 122
 Leucine rich repeat kinase 2 (LRKK2), 348
 Leukoaraiosis, 443, 444
 Leukocoria, 672
 Levodopa (L-DOPA), 47, 425
 Limb dysmetria, 238
 Limbic encephalitis (LE), 611–613
 autoimmune epilepsy, 511, 513–515
 etiology, 511
 infectious/viral, 511
 Limbic-Predominant Age-Related TDP-43 Encephalopathy (LATE), 305
 Line of response (LOR), 4, 27, 29
 Linear Discriminant Analysis (LDA)-based classifier, 154
 Logopenic variant primary progressive aphasia (lvPPA), 253, 313
 amyloid PET, 316, 318, 319
 clinical presentation, 313–315
 clinical symptoms, 320
 disease genetics, 320
 epidemiology, 313
 ¹⁸F-FDG PET, 315, 316
 pathology-supported diagnosis of lvPPA, 319, 320
 structural imaging, 315
 treatment, 320
 Lower motor neurons (LMNs), 397, 473
 Lumboperitoneal (LP) shunt, 464
 Lung cancer, 660
 Luxury perfusion, 208
 Lymphadenopathy, 701
 Lymphoma, 679–681, 690, 718, 719

M

Machine learning techniques, 532
 Mad cow disease, 387
 Magnetic resonance spectroscopy (MRS)
 modifiable daily lifestyle behaviors, 61
 obesity, 58
 Magnetization Prepared – Rapid Gradient Echo (MPRAGE), 20
 Major depressive disorder, 193

Malformation of cortical development (MCD), 499, 742, 745
 Malignant peripheral nerve sheath tumors (MPNSTs), 769
 Marker tracking systems, 80, 81
 Mean absolute error (MAE), 85
 Mean transit time (MTT), 830
 Medial temporal lobe (MLT) tracer, 112
 Medulloblastoma (MB), 221, 550
 Meningiomas, 217, 218, 554, 558, 716
 Mesial temporal sclerosis (MTS), 507, 508, 746–748
 Metabolic changes, AIS, 207, 208, 231
 Metastatic disease, 223
 brachial plexus, 663
 breast cancer, 660
 cerebral hemisphere, 565
 clinical practice, 565
 clinical symptoms, 565
 contrast-enhanced MRI, 565, 566
 cutaneous melanoma, 657, 658
 definition, 657
 dural metastases, 565
 extra-axial metastases, 569, 571
 facial bones, 663
 FDG PET, 571, 574
 gastrointestinal cancer, 660, 661
 genitourinary cancer, 660, 661
 hematogenous metastases, 658
 intraparenchymal metastases, 566, 569
 leptomeningeal metastases, 565
 lesion conspicuity, 566
 lung cancer, 660
 lymphatic metastasis, 658, 659
 mucosal melanoma, 658
 in neck PET/MRI
 anatomic imaging, 664
 evaluation, 664, 665
 limitations, 667
 primary neoplasm, 666
 radiation planning, 667
 recurrence, 665
 treatment assessment, 665, 666
 ultrasound-guided fine needle aspiration, 664
 nodal metastases, 658, 659
 non-FDG PET, 574, 575
 oral cavity, 662
 orbital metastases, 660, 662
 paranasal sinuses, 663
 parathyroid glands, 662
 parenchymal metastases, 660, 662
 primary malignancy, 657
 salivary gland, 662
 salivary gland neoplasms, 658
 somatostatin receptor PET imaging, 667
 thyroid, 662
 Methionine homozygous (MM), 388
 Microdialysis studies, 179
 Microglial activation, 368
 Alzheimer's disease, 193
 clinical application, 193
 image interpretation, 192
 18 kDa translocator protein, 191
 major depressive disorder, 193
 neuroinflammation, 191
 neuroinflammatory proteins, 192
 PET radiotracers, 191, 192
 PET/MRI modalities, 194
 traumatic brain injury, 194

- Microtubule Associated protein tau (MAPT) gene, 348
Mild cognitive impairment (MCI), 105, 180
Mini-Mental State Examination (MMSE), 233
Mitochondrial encephalopathy, lactic acidosis and stroke-like episodes (MELAS), 811–813
Modic classification, 724
Modifiable daily lifestyle behaviors
 arterial spin labeling, 60
 connectivity, 61
 diet, 59
 diffusion tensor imaging, 61
 glymphatic Imaging studies, 61, 62
 magnetic resonance spectroscopy, 61
 physical activity, 59
 volume, 60
Modified Boston Criteria, 273
Molecular imaging
 applications
 amyloid/tau imaging, 52–55
 homeostasis (defense and repair), 50, 52, 53
 metabolism (synthesis and perfusion), 48–50
 perfusion, 50, 51
 signaling and transport, 46–48
 smart contrast agents, 45, 46
Monoamine oxidase B (MAO-B), 192
Montreal cognitive Assessment (MoCA), 234
Motion correction, 80, 81
 advantages, 29, 33
 custom-molded headcase, 27
 disadvantages, 29, 33
 gated PET motion correction techniques, 29
 head motion, 27
 head restraints, 27
 lines or response, 27, 29
 motion blurred and PET brain image, 27
 MR-assisted motion correction, 30
 MR hardware, 30, 31
 MR image-based motion correction methods, 31, 32
 MR navigator correction methods, 32
 optical tracking systems, 29
 PET fiducial marker-based approaches, 30
 PET motion correction algorithms, 27
Motor symptoms, 228
Moyamoya disease (MMD), 814–816, 818–821
Moyamoya syndrome (MMS), 814–816, 818–821
MR-assisted motion correction, 30
 MR hardware, 30, 31
 MR image-based motion correction methods, 31, 32
 MR navigator-based motion correction, 32
MR-based attenuation correction (MR-AC), 19, 21, 37
MR hardware-based approaches, 31
MRI component, 4
MR image-based motion correction methods, 31, 32
MR navigator-based motion correction, 32
Mucoepidermoid carcinoma, 690
Mucosal melanoma, 658
Multi system atrophy (MSA), 230
Multi-infarct dementia (MID), *see* Vascular cognitive impairment (VCI)
Multi-modal neuroimaging-based studies, 81
Multimodality DL models function, 70
Multiple myeloma (MM), 717, 718
Multiple sclerosis (MS), 729
 disease progression, 617
 functional imaging, 617, 618
 hybrid PET-MRI imaging, 618, 619
 overview, 617
 structural imaging, 617
Multiple system atrophy (MSA), 421
 clinical features, 362
 diagnosis, 362
 epidemiology, 361
 magnetic resonance imaging, 362, 363
 MSA-C, 363, 365–367
 MSA-P, 363–365
 pathophysiology, 361, 362
 positron emission tomography
 cholinergic system, 367, 368
 dopaminergic system, 366, 367
 glucose hypometabolism, 366, 368
 microglial activation, 368
 Tau deposits, 368, 369
 treatment, 370
Myxopapillary ependymoma, 769
- N**
Na⁺-dependent transporters, 137
Nasopharyngeal carcinoma (NPC), 629, 631, 648, 650
Neoplasms, 503–505
Neural tube defects, 723
Neuroblastoma, 757, 759, 760, 771, 772, 774
Neurodegenerative disease, 91, 92, 248
 Alzheimer's disease, 248
 behavioral variant of a frontotemporal dementia, 252
 dementia with Lewy bodies, 250
 dementias with motor variants, 250, 251
 language variants of frontotemporal dementia, 252
 Parkinson's disease dementia, 250
 posterior cortical atrophy, 249
 primary progressive aphasia, 253
Neurofibroma, 683
Neurofibromatosis 1 (NF 1), 769
Neuroinflammation
 amino acid tracers, 599–601
 diagnosis, 599
 imaging patterns, 602
 TSPO, 599
Neurologic evaluation
 (amyloid, tau, neurodegeneration) ATN system, 242
 cranial nerves, 236
 acoustic and vestibular function, 236
 eye and fundus oculi exam, 236
 oculomotor function, 236
 olfaction, 236
 trigeminal and facial nerves, 236
 visual field testing, 236
 dystonia, 238
 family history, 232
 general medical exam, 239
 cardiovascular and respiratory system, 239
 habitus and appearance, 239
 head and neck, 239
 musculoskeletal and skin changes, 240
 imaging, 240–242
 laboratory tests, 240
 limb dysmetria, 238
 medical history
 age of onset, 228
 appetite changes, 230
 autonomic changes, 230
 Neurologic evaluation (*cont.*)

- behavioral changes, 229
- bowel and bladder habits changes, 230
- cerebrovascular disease, 228
- confabulations, 229
- corticobasal degeneration, 228
- COVID-19 pandemic, 230
- depression, 229
- episodic memory defects, 228
- hallucinations, 229
- history of present illness-clinical presentation, 228, 229
- Huntington disease, 228
- motor symptoms, 228
- obstructive sleep apnea, 229
- retrograde amnesia, 228
- short term memory defects, 228
- sleep alterations, 229
- spatial disorientation, 228
- temporal disorientation, 228
- verbal and physical aggression, 229
- Wilson's disease, 228
- medications
 - antidepressants-tricyclic antidepressants, 232
 - antihistamines, 232
 - antipsychotics/antidopaminergics, 232
 - benzodiazepines and hypnotics, 233
 - muscle relaxants, 233
 - pain relief medications, 233
 - peripheral alpha-1 blockers/central alpha agonists, 232
- mental status exam
 - agnosia, 235
 - alertness, 233
 - arousal, 233
 - attention, 234
 - constructional praxis, 235
 - dressing, 235
 - dynamic praxis, 235
 - frontal functions, 234
 - ideational praxis, 235
 - ideo-motor praxis, 235
 - language, 234
 - memory, 234
 - motor praxis, 234
 - orientation, 234
 - praxis, 234
 - visuospatial function, 234
 - wakefulness, 233
- motor system and gait
 - axial instability, 237
 - involuntary movements tremor, 237
 - segmental strength, 236
 - stance and gait exams, 237
 - tone, 237
- past medical and surgical history
 - autoimmune encephalitis, 231
 - cancer, 231
 - cardiovascular risk, 230
 - immunological disease, 231
 - metabolic changes, 231
 - obstructive sleep apnea, 230
 - psychiatric illnesses, 231
 - recent and prolonged surgeries, 231
 - thyroid disease, 231
 - traumatic brain injury, 231
- pathology, 242
- psychiatric symptoms
 - anxiety, 235
 - depression, 235
 - pseudobulbar affect, 236
 - psychotic symptoms, 235
 - sensory system, 238
 - social history, 232
- Neuronal and mixed neuronal-glia tumors, 546
- Neuro-oncology, 74, 75, 92
 - brain tumors, 92
 - FDOPA
 - aminoacid tracer, 121, 122
 - and PET/MRI, 123
 - image interpretation, 122
 - indications, 96
 - limitation, 92
 - limitations, 96, 97
 - treatment response evaluation, 95, 96
 - tumor diagnosis and grade, 92–95
- Neuropsychology
 - assessment, 247
 - cognitive functioning, 247
 - definition, 247
 - evaluation, 247
 - hybrid neuroimaging, 254
 - neurodegenerative disease, 248
 - Alzheimer's disease, 248
 - behavioral variant of a frontotemporal dementia, 252
 - Dementia with Lewy bodies, 250
 - dementias with motor variants, 250, 251
 - language variants of frontotemporal dementia, 252
 - Parkinson's disease dementia, 250
 - posterior cortical atrophy, 249
 - primary progressive aphasia, 253
- Neurovascular unit (NVU), 839
- Nigrostriatal pathway, 366
- ¹[N-methyl-C-11]α-Methylaminoisobutyric acid ([¹¹C]-MeAIB), 146
- Nonfluent/agrammatic variant primary progressive aphasia (nfvPPA), 313
 - clinical presentation, 337, 338
 - disease genetics, 343
 - epidemiology, 337
 - functional and molecular imaging, 339, 340, 342–344
 - neuroimaging abnormality patterns, 338
 - pathology, 343
 - structural imaging, 338, 339
 - treatment, 344
- Nongerminomatous tumors, 557
- Non-invasive dynamic method, 198
- Non-invasive steady-state method, 198
- Normal pressure hydrocephalus (NPH)
 - advanced MR imaging, 463
 - CAPPAH sign, 464
 - clinical diagnosis, 460
 - conventional MRI, 460, 461, 463
 - callosal angle, 461
 - DESH, 461
 - Evans index, 461
 - volumetric analysis, 461, 462
 - CSF biomarkers, 460
 - CSF flow studies, 463
 - CSF tap test, 460
 - etiology, 459
 - positron emission tomography, 461–464
 - radionuclide cisternography, 464
 - treatment, 464, 465
- Nuclear brain imaging technique, 167
- Numerous cortical cerebral microhemorrhages, 274

O

Obesity

- and aging brain, 58
- arterial spin labeling, 58
- connectivity, 59
- diffusion tensor imaging, 59
- glymphatic imaging, 59
- magnetic resonance spectroscopy, 58
- prevalence, 57
- risk factor, 57
- volume, 58

Obesity paradox, 57

Obstructive sleep apnea (OSA), 229, 230

Occipital hypoperfusion, 297

Ocular adnexal lymphoma (OAL), 679–681

O-(2-[¹⁸F]fluoroethyl)-L-tyrosine ([¹⁸F]-FET), 146

- biochemical characteristics, 146
- dynamic, 147, 150, 151
- early response to treatment, 151, 152
- machine learning, 154
- non-invasive genetic profiling, 153
- photopenic defect, 153, 154
- static, 147
- tumor genotyping, 153
- tumor grading, 151
- tumor progression vs. treatment-related changes, 152, 153
- unique feature of, 146

Oligodendroglial alpha-synuclein, 361

Oligodendrogliomas (ODG), 144, 540, 541

¹⁵O PET imaging

- aging and neurodegeneration, 209, 210
- arterial spin labeling (ASL) methods, 198
- cerebrovascular disease
 - cerebral hemodynamics, 201, 203–205, 207
 - intracerebral hemorrhage, 209–211
 - metabolic changes, 207, 208
 - tissue function and viability, 208, 209
- dynamic and steady-state methods, 197
- dynamic susceptibility contrast method, 198
- IDAIF methods, 198
- non-invasive dynamic methods, 198
- non-invasive steady-state method, 198
- normal physiology and functional imaging, 198–206
- OEF method, 198

Optic nerve glioma (ONG), 674, 675

Optic nerve sheath meningioma (ONSM), 675, 676

Optical tracking-based motion correction, 29

Orbital tumors

- cavernous malformation, 676–678
- IOP, 679
- lacrimal gland masses, 682, 683
- lymphoma, 679–681
- metastatic lesions, 681
- multiparametric MRI, 685
- ocular compartment, 671
- ONG, 674, 675
- ONSM, 675, 676
- peripheral nerve sheath tumor, 683
- PNTS, 685
- retinoblastoma, 672
- RMS, 678, 679
- sinonasal and skull base malignancies, 684
- uveal melanomas, 673, 674
- VLM, 683

Ordered Subsets Expectation Maximization (OSEM) reconstruction methods, 80

Oropharyngeal squamous cell carcinoma (OPSCC), 644, 648

Orthogonal 2D spiral navigators, 32

Osteomyelitis, 772, 774, 775

Osteoporosis, 724, 725

Oxygen extraction fraction (OEF), 451

P

Papillary tumor of pineal region (PTPR), 555

Paragangliomas (PGLs), 218, 220, 716, 718

Parkinson plus syndromes, 373

Parkinson's disease (PD), 124

- atypical parkinsonian syndromes, 73
- clinical features, 421
- early diagnosis, 70–72
- early differentiation of, 73, 74
- dopaminergic imaging
 - normal imaging, 425
 - postsynaptic imaging, 425, 426
 - presynaptic function, 423–425
- genetic risk factors, 421
- magnetic resonance imaging, 421, 422
- metabolic imaging
 - abnormal network architecture, 430
 - APS, 430, 431
 - cognition-related pattern, 428
 - network analysis, 428–430
 - PD-related motor pattern, 426, 427
 - preclinical PD, 426, 427
 - treatment-related network imaging, 431
 - tremor, 427, 428

microglial activation, 432

pathological hallmark, 421

serotonergic imaging, 431, 432

transcranial sonography, 422, 423

Parkinson's disease dementia (PDD), 228, 250

Parkinson's disease-related pattern (PDRP), 426, 427

Parkinsonian syndrome, 228

Partial response (PR), 590

Partial volume effects (PVE), 106

Peak signal-to-noise ratio (PSNR), 85

Pediatric brain tumors

- amino acid transport, 754, 755, 757
- ¹⁸F-fluoro-ethyl-tyrosine PET, 753–756
- head and neck malignancies, 755, 756
- neuroblastoma, 757, 759, 760
- non-oncologic applications, 761–763
- orbital malignancies, 756
- primary diagnosis, 753
- rhabdomyosarcoma, 756–760
- standard of care treatment, 753
- thyroid cancer, 761

Pediatric epilepsy

- diagnostic accuracy, 742
- FCD, 741–743, 745
- hemispheric abnormalities, 750
- hypometabolism, 743, 746
- metabolic imaging, 741
- optimization, 741
- posterior frontal MCD, 742, 745
- structural abnormalities, 742, 744
- TLE, 746–749
- TSC, 748–750

Pediatric PET/MRI imaging

- clinical studies, 737
- cost analysis, 739
- diffusion weighted images, 737
- dose reduction, 737

- Pediatric PET/MRI imaging (*cont.*)
 fluid attenuation inversion recovery images, 737
 protocols, 739
 sedation, 737, 738
 sensitivity for detection, 737
 sequences, 737, 738
 synchronous system, 737
- Pediatric spine tumors
 astrocytoma, 765–767
 ependymoma, 766–768
 Ewing sarcoma, 769, 770
 extradural tumors, 769
 LCH, 771, 773
 lymphoma, 770, 772, 773
 MPNSTs, 769
 neuroblastoma, 771, 772, 774
 PERCIST, 765
 peripheral nerve sheath tumors, 766–768
 posterior fossa tumors, 769
 SCT, 769, 771
 spinal cord neoplasms, 765, 766
- Pediatric temporal lobe epilepsy (TLE), 746–749
- Perfusion imaging
 ASL, 839, 840
 BBB, 839
 DCE, 841
 DSC, 840, 841
 neurodegenerative disease, 846, 847
 neuro-oncology, 842, 844–846
 neurovascular disease, 841–843
 NVU, 839
- Perineural tumor spread (PNTS), 685, 699, 700
- Peripheral nerve sheath tumor, 683, 766–768
- Perivascular spaces (PVS), 444
- PET amyloid tracers, 99
- PET fiducial marker-based approaches, 30
- PET motion correction algorithms, 27
- PET/MRI systems
 components, 6
 detector design considerations, 5
 DOI measurement, 4
 gamma-ray acollinearity, 3
 line of response, 4
 magnetic susceptibility, 6
 vs. medical imaging modalities, 3
 normal/pathological molecular states/processes, 3
 picomolar concentration of ligand, 3
 pulse of radiofrequency radiation, 5
 quantification, 7
 quantum mechanical property, 5
 RF shielding, 6
 with single tracer molecule, 3
 SiPM designs, 5
 system geometry and implications, 6
 time-of-flight (TOF) capability, 4, 5
- P-glycoprotein (P-gp), 168
- Phase difference enhanced imaging (PADRE), 398
- Phosphodiesterase 10A (PDE10A), 416
- Pick's disease, *see* Behavioral variant frontotemporal dementia (bvFTD)
- Pilocytic astrocytomas (PA), 545
- Pineal parenchymal tumors, 555
- Pineal tumors, 554
- Pineoblastomas, 555
- Pineocytomas, 555
- Pineocytomas, pineal parenchymal tumor of intermediate differentiation (PPTID), 555
- Pituitary adenomas, 221, 222, 554
- Pleomorphic adenoma, 690
- Pleomorphic xanthoastrocytomas (PXA), 546
- Plexiform neurofibroma, 683, 767, 768
- Point-spread function (PSF), 3
- POLARIS, 29
- Positron Emission Tomography Response Criteria in Solid Tumors (PERCIST), 765
- Posterior cortical atrophy (PCA), 249
 clinical features, 284
 epidemiology, 283, 284
 neuroimaging feature, 284
 functional imaging, 285, 287, 288
 structural imaging, 284
 pathologic features and biomarkers, 288
 treatment, 288
- Post-synaptic ligands, 297
- Prefrontal hypoperfusion, 297
- Prelaryngeal node, 658, 659
- Presenilin 1 (PS1), 481
- Presynaptic ligands, 295, 297
- Primary angiitis of the CNS (PACNS), 621, 622
- Primary brain neoplasms
 astrocytic tumors
 desmoplastic infantile tumors, 548
 dysembryoplastic neuroepithelial tumor, 547
 dysplastic cerebellar gangliocytoma, 548
 embryonal tumors, 548, 550
 gangliocytomas, 547
 gangliogliomas, 547
 neuronal and mixed neuronal-glia tumors, 546
 pilocytic astrocytomas, 545
 diffuse gliomas, 540
 diffusely infiltrating gliomas
 astrocytoma, IDH-mutant, 541, 542
 diffuse midline glioma, H3K27M-mutant, 543
 glioblastoma multiforme, 542, 543
 oligodendrogliomas, 541
 imaging approach and techniques, 539
 intraventricular masses
 central neurocytoma, 552
 chordoid and glial elements, 554
 choroid plexus tumors, 552
 CNS lymphoma, 559
 craniopharyngiomas, 554
 ependymal tumors, 550, 551
 extra-axial tumors, 557
 germ cell tumors, 555
 germinomas, 557
 hemangioblastomas, 559
 hemangiopericytoma/solitary fibrous tumor, 558
 hypothalamic/chiasmatic astrocytoma, 554
 langerhans cell histiocytosis, 560
 meningiomas, 554, 558
 nongerminomatous tumors, 557
 pineal parenchymal tumors, 555
 pineal tumors, 554
 pituitary adenomas, 554
 primary melanocytic lesions, 559
 sellar/ central skull base region, 554
 pleomorphic xanthoastrocytomas, 546
 WHO classification, 539
 WHO grading, 540

- Primary lateral sclerosis (PLS), 397
- Primary melanocytic lesions, 559
- Primary progressive aphasia (PPA)
- clinical cases, 253
 - logopenic (lvPPA) variant
 - amyloid PET, 316, 318, 319
 - clinical presentation, 313–315
 - clinical symptoms, 320
 - disease genetics, 320
 - epidemiology, 313
 - ¹⁸F-FDG PET, 315, 316
 - pathology-supported diagnosis of lvPPA, 319, 320
 - structural imaging, 315
 - treatment, 320
 - nonfluent/agrammatic variant
 - clinical presentation, 337, 338
 - disease genetics, 343
 - epidemiology, 337
 - functional and molecular imaging, 339, 340, 342–344
 - neuroimaging abnormality patterns, 338
 - pathology, 343
 - structural imaging, 338, 339
 - treatment, 344
- PPA-G, 253
- PPA-L, 253
- PPA-S, 253
- semantic variant
- clinical presentation, 323, 324
 - diagnostic criteria, 324
 - disease genetics, 327, 328
 - epidemiology, 323
 - functional imaging, 325
 - molecular imaging, 325, 328, 329, 333
 - pathology, 327
 - structural imaging, 324–326
 - treatment, 328
- Principal component analysis (PCA), 427
- Probabilistic neural networks (PNNs), 70
- Progressive disease (PD), 591
- Progressive supranuclear palsy (PSP), 250, 251, 421
- age of onset, 348
 - clinical clues, 348
 - clinical subtypes, 347
 - disease course, 348
 - genetic or environmental factors, 348
 - histopathologic diagnostic criteria, 348
 - history, 347
 - imaging, 348
 - imaging features
 - CT, 352
 - DAT SPECT, 352
 - DWI and ADC, 352
 - ¹⁸F-FDG-PET, 353, 354
 - MRI, 348, 349, 351, 352
 - PET, 353
 - tau PET, 354, 355
 - imaging, role of, 347
 - incidence, 347
 - LRKK2 mutation, 348
 - MAPT gene, 348
 - subtypes, 348
 - treatment, 355
- Prostate cancer, 660, 661
- Pseudobulbar affect, 238
- Pseudoprogession, 95
- Psychiatric illnesses, 231
- Pulvinar sign, 805
- ## Q
- Quantitative susceptibility mapping (QSM), 398–400, 495
- Quantitative accuracy, 80
- Quantitative PET analysis
- dynamic, 22–24
 - static, 21, 22
- ## R
- Radial diffusivity (RD), 787
- Radiation-induced spinal complications, 730, 731
- Radiculomyelitis, 728
- Radioactive Drug Research Committee (RDRC) application, 13, 14
- Radiogenomics, 532
- Radiolabeled somatostatin receptor (SSTR), 531, 532
- Radiomics, 532
- Radionuclides, 67
- Radiopharmaceutical development, 67
- chemical design, 9, 10
 - clinical diagnosis, 9
 - early clinical testing, 14
 - in vitro tracer validation, 11, 12
 - in vivo tracer evaluation, 12, 13
 - isotope selection, 10, 11
 - RDRC and IND applications, 13, 14
 - regulatory control, 13
 - typical approach, 9, 10
- RANO-brain metastases (RANO-BM), 592, 593
- RANO-leptomeningeal metastases (RANO-LM), 593, 594
- Rapidly progressive dementias (RPDs), 118
- Rasmussen's encephalitis, 750
- Reactive degenerative changes, 724
- Real-time quaking-induced conversion (RT-QuIC) assay, 387
- Reduction in relative CMRglu (rCMRglu), 450
- Regional binding pattern, 101
- Regional cerebral blood flow (rCBF), 198
- Regional cerebral metabolic rate of glucose (rCMRglc), 198, 199
- Regional cerebral metabolic rate of oxygen (rCMRO₂), 198
- Regional glucose impairment, 89
- Regional neuronal activity, 92
- Relative cerebral blood volume (rCBV), 569
- REM sleep behavior disorder (RBD), 421, 424, 426
- REM sleep movement disorder, 293
- Response assessment in neuro-oncology (RANO)
- advanced MRI techniques and PET, 594, 595
 - brain metastases, 592, 593
 - iRANO, 593
 - leptomeningeal metastasis, 593, 594
 - RANO-high grade glioma
 - complete response, 589
 - limitations, 589
 - partial response, 590
 - progressive disease, 591
 - pseudoprogession, 591
 - pseudoresponse, 591, 592
 - radiation necrosis, 591
 - stable disease, 590
 - target lesions, 589, 590
 - RANO-low grade glioma, 592
 - RAPNO, 594
- Response assessment in pediatric neuro-oncology (RAPNO), 594

- Resting-state fMRI (rs-fMRI), 309, 310
 Retinal vasculopathy with cerebral leukodystrophy with systemic manifestations (RVCL-S), 810, 811
 Retinoblastoma, 672
 Retrograde amnesia or fluctuating symptoms, 228
 Rhabdomyosarcoma, 756–760
 Rhabdomyosarcoma (RMS), 678, 679
 Richardson syndrome (RS), 347
 Rosai-Dorfman disease (RDD), 761, 763
- S**
- Saccular aneurysms, 795
 Sacrococcygeal teratomas (SCT), 769, 771
 Salivary gland tumor
 benign tumor, 690, 692, 694
 clinical presentation, 689
 developments, 706
 distant metastases, 701
 imaging
 differentiation, 701
 dynamic contrast enhanced (DCE) MR imaging, 702
 18-fluorodeoxyglucose-PET imaging, 703–705
 hybrid PET/MR, 705, 706
 magnetic resonance imaging, 702, 703
 preoperative characterization, 702
 ultrasound, 702
 imaging features, 694–697
 lymphadenopathy, 701
 malignant tumor, 690
 non-neoplastic pathologies, 697
 parotid glands, 689, 690
 PNTS, 699, 700
 staging, 697, 699
 Sarcoidosis, 613–615, 729, 730
 Scans without evidence of dopaminergic deficit (SWEDD), 70
 Schwannoma, 683, 715, 716
 Secondary CNS vasculitis, 622, 623
 SEGBONE method, 21
 Selective serotonin reuptake inhibitors (SSRIs), 167
 Sellar/ central skull base region, 554
 Semantic variant of PPA (PPA-S), 253
 Semantic variant primary progressive aphasia (svPPA)
 clinical presentation, 323, 324
 diagnostic criteria, 324
 disease genetics, 327, 328
 epidemiology, 323
 functional imaging, 325
 molecular imaging, 325, 328, 329, 333
 pathology, 327
 structural imaging, 324–326
 treatment, 328
 Semiquantitative standardized uptake value ratios (SUVRs), 101
 Serotonergic system, 167
 Serotonin (5-hydroxytryptamine [5-HT]), 167
 brain imaging, 167, 168
 5-HT1 receptors, 168, 169
 5-HT2 receptors, 169, 170
 5-HT3 receptors, 170
 5-HT4 receptors, 170
 5-HT5 receptors, 170
 5-HT6 receptors, 170
 5-HT7 receptors, 171
 Serotonin reuptake transporter (SERT), 171
 Siemen's 3D PACE motion correction, 32
 Silicon photomultiplier (SiPM), 5
 Simplified reference tissue model (SRTM) three-compartment system, 22
 Single tracer molecule, 3
 Sjögren syndrome, 697
 Skull base tumors, 581, 584
 Small vessel disease (SVD)
 CMB, 789, 790
 computed tomography, 785
 diffuse weighted imaging, 787
 diffusion tensor imaging, 787
 dynamic contrast enhanced MRI, 789
 epidemiology, 781
 functional MRI, 787
 hyperhomocysteinemia, 790, 791
 magnetic resonance imaging, 785, 787
 MR spectroscopy, 787
 neuroimaging biomarkers, 782
 pathophysiology, 782
 risk factor, 781, 782
 treatment and management, 789
 Small vessel ischemic disease (SVID), 444
 Solitary fibrous tumors, 558
 Spinal dysraphisms, 723
 Spinal infections
 bacterial spondylodiscitis, 726, 727
 factors, 725
 functional imaging, 728
 fungal infections, 726
 septic arthritis, 726, 727
 structural imaging, 726
 Spinal neoplasms
 intradural extramedullary neoplasm, 715–718
 intramedullary neoplasm
 astrocytoma, 714
 ependymoma, 713–715
 hemangioblastoma, 714
 metastases, 714–716
 symptom, 713
 lymphoma, 718, 719
 multiple myeloma, 717, 718
 osseous metastases, 719, 720
 primary osseous neoplasms, 719
 Spinal tuberculosis, 728
 Spoiled gradient-recalled echo (SPGR), 20
 Square wave jerks, 239
 Stable disease (SD), 590
 Standardized uptake value ratio (SUVr), 22, 181, 473
 Standards for Reporting Vascular Changes on Neuroimaging (STRIVE), 785
 Statistical parametric mapping (SPM), 309, 473
 Stroke, 441
 Structural connectivity, 59
 Structural similarity index measure (SSIM), 85
 Sturge-Weber syndrome, 499, 501
 Subcortical ischemic vascular cognitive impairment (SI-VCI), 447–448
 Subependymomas, 550
 Substantia nigra hyperechogenicity, 422, 423
 Superficial siderosis, 275
 Susceptibility-weighted imaging (SWI), 398–400
 System L transporters, 137, 138
 Systemic lupus erythematosus (SLE), 615
- T**
- Tailored psychoeducation programs, 288
 Tau imaging

in Alzheimer's disease, 115–117
 clinical applications, 113, 114
 flortaucipir PET images, 112, 113
 Lewy body dementia, 117
 medial temporal lobe tracer, 112
 multiple system atrophy, 368, 369
 non-AD tauopathy, 117
 Parkinson's disease, 117
 PET tracers, 111, 112
 PET/MR imaging, 118
 progressive supranuclear palsy, 354, 355
 Tau neurofibrillary tangles, 288
 Temporal lobe epilepsy (TLE), 507, 508
 Three-repeat (3R) isoform tau, 304
 Thyroid cancer, 761
 Thyroid disease, 231
 Time activity curve (TAC), 22, 146
 Time-of-flight (TOF) capability, 4, 5
 2 tissue-compartment (TC) model, 23
 Toft and Kermode (TK) model, 854
 Toxic cytoplasmic protein, 411
 Toxoplasmosis, 602, 604, 605
 Tracer doses, 3
 Tract-based spatial statistics (TBSS), 446, 447
 Transcranial sonography (TCS), 422, 423
 Translocator protein (TSPO), 406, 416, 599
 Traumatic brain injury (TBI), 194, 231
 amyloid and tau deposits, 485
 big data and machine learning, 487
 brain metabolites, 487
 causes, 479
 classification, 479, 480
 computed tomography, 483
 CTE, 481
 definition, 479
 diffusion tensor imaging, 483
 economic burden, 479
 epidemiology, 479
 excitotoxicity, 487
 [18F]-fluorodeoxyglucose, 484–486
 functional magnetic resonance imaging, 484
 head trauma, 480
 hybrid PET/MR scanners, 487–489
 hypoxia and oxidative stress, 487
 magnetic resonance imaging, 483
 magnetic resonance spectroscopy, 483, 484
 neuroinflammation imaging, 485
 pathophysiology, 480–482
 perfusion imaging, 484
 tau-PET imaging, 485
 Traumatic encephalopathy syndrome (TES), 481
 Treatment-related changes (TRC), 95, 144
 True baseline theory, 200
 Tuberous sclerosis (TSC), 500, 502, 503, 748–750
 Tumor-to-background (TBR) ratio, 94

U

Ultra-short echo time (UTE) sequence, 19, 80
 Undifferentiated carcinomas (UC), 629

Unified Parkinson's disease rating scale (UPDRS), 424, 426
 United Imaging Healthcare (UIH), 30
 Upper motor neurons (UMNs), 397, 473
 Urinary incontinence, 460
 Urinary urgency, 460
 Uveal melanomas, 673, 674

V

Variant CJD (vCJD), 387
 Vascular cognitive impairment (VCI), 785
 computerized tomography, 443
 diabetes mellitus, 454
 diffusion tensor imaging, 444–448
 diffusion weighted imaging, 444
 dynamic contrast-enhanced MR imaging, 448, 449
 epidemiology, 441–443
 functional MR imaging, 451
 hypercholesterolemia/dyslipidemia, 454
 hypertension, 453, 454
 magnetic resonance imaging, 443–446
 MR spectroscopy, 447–449
 neuronal networks, 451–453
 non-pharmacological measures, 454
 pharmacological management, 452, 453
 positron emission tomography, 450, 451
 Vascular dementia (VaD), *see* Vascular cognitive impairment (VCI)
 Vascular malformation
 arteriovenous malformation, 798, 799
 capillary telangiectasias, 802
 cerebral cavernous venous malformation, 801, 802
 DAVF, 800
 DVA, 801
 Vascular mild cognitive impairment (VaMCI), 451
 Venolymphatic malformation (VLM), 683
 Ventriculoperitoneal shunt (VPS), 464
 Vesicular acetylcholine transporter (VACHT), 184, 185
 Vesicular monoamine transporter 2 (VMAT2), 47, 366
 Video camera surveillance system, 29
 Virchow Robin (VR), 444
 Volumetrics
 modifiable daily lifestyle behaviors, 60
 obesity, 58

W

Waldeyer's lymphoid tissue, 629, 631
 Warburg effect, 89
 Water- and fat-suppressed proton projection imaging (WASPI)
 sequence, 20
 White matter hyperintensities (WMH), 443, 444
 Whole-body PET/MRI systems, 7
 Wilms tumor, 756
 Wilson's disease, 228
 Working memory, 234

Z

Zero echo-time (ZTE) sequences, 19, 80